2

From Natural System to Numerical Model

Natural geological systems are generally highly complex, both as far as the geological structure and the physical processes occurring within them are concerned. In order to investigate such systems, it is necessary to understand the natural processes, their interaction with the geological structure and their relative importance on different problem scales.

Due to the geometrical complexity of the natural system and the large number of physical processes involved, it is not feisable to describe the exact system in great detail. The system structure and the processes occurring within it are therefore represented by conceptual models, designed to meet the requirements of certain types of problems on a given scale. This implies, for example, the introduction of parameters representing the material properties and of physical descriptions of the relevant flow and transport processes.

In order to solve a problem, a mathematical description of the model concept is required. Due to the degree of complexity of this type of problem, analytical solutions are not an option. The numerical solution involves the spatial and the temporal discretization of the problem and the use of efficient and stable numerical algorithms.

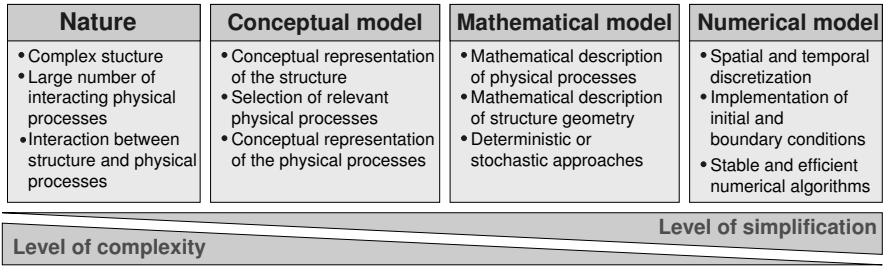

Fig. 2.1. Transformation from a complex natural system to a simplified numerical model (Süß, 2004).

The transformation of a natural system to a model inevitably leads to simplifications of the real system as visualized in Fig. 2.1. When model results are being interpreted, it is therefore essential to keep in mind that a model is merely an approximation of nature. One must always be aware of the assumptions and the concepts used for a specific model in order to assess its results correctly.

This chapter describes the transformation from nature to model of saturated fractured porous systems as well as the flow and the transport processes that are relevant for the investigations discussed in this book. The first part (Sect. 2.1) deals with the characteristics of natural fractured porous systems. This is followed by a discussion of different model concepts used on different scales and for different problem types (Sect. 2.2). Finally, the governing equations of the pertinent physical processes and the mathematical implementation of the discussed model concepts are presented (Sects. 2.3 – 2.5). It should be underlined that this chapter does not provide a complete overview of physical processes, theories, concepts and models. It is restricted to the scope of the research work presented in this book. For a more detailed discussion of the topic, we refer to the literature references given in the various sections.

2.1 Natural Fractured Porous Systems

A. Silberhorn-Hemminger, M. Süß, R. Helmig

Solid rock can be classified according to its diagenetic characteristics (Kolditz, 1997). Consolidated sedimentary rock evolves from the cementation of mineral grains, metamorphic rock is the result of recrystallization under high temperature and stress whereas igneous rock forms by the direct crystallization of minerals from magmaic melt.

In direct response to the stress applied, which may be lithostatic, tectonic, thermal or the result of high fluid pressures, joints, faults and systems of such discontinuities occur on different scales and with different geometries. Tectonic fractures tend to be oriented along stress fields on a regional scale, whereas the other types of stresses give rise to local fractures that vary more greatly in orientation. Apart from stress-induced fractures, joints may also occur at the boundaries of sedimentary layers consisting of deposits of different properties. The properties of existing fractures can be altered by local physical and chemical processes. In hydrogeology, the term *fractures* is often used for all the different types of discontinuities (e.g. faults or fissures) in the rock matrix.

Figure 2.2 shows an exposed vertical wall of fractured sandstone containing both vertical and horizontal fractures. In this case, the horizontal fractures are separation planes between different sedimentary layers, whereas the vertical fractures are the result of mechanical stress.

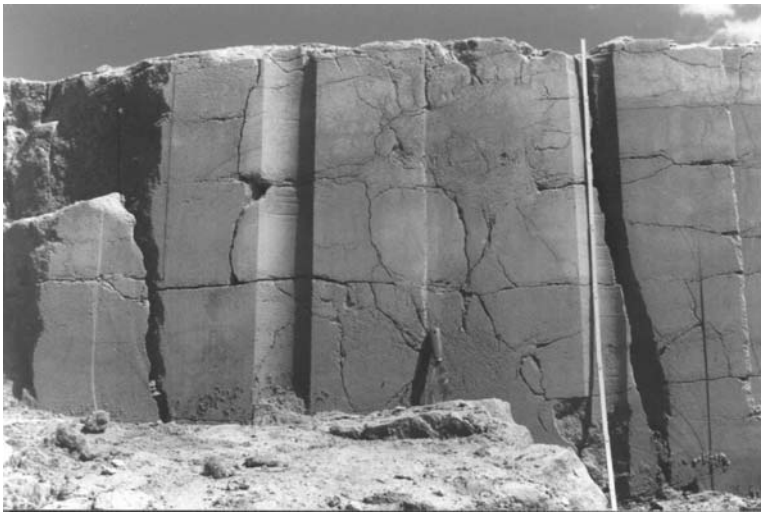

Fig. 2.2. Vertical exposed wall of fractured sandstone at the field site (Sect. 5).

The hydraulic properties of hard rock are to a large extent determined by the porosity of the rock. Table 2.1 presents typical ranges of porosity for different types of hard rock, considering the rock as a whole, including both fractures and matrix (see below). Depending on the type of rock, the contribution of these two components to the porosity varies. For example for granite, the porosity is almost exclusively determined by the fractures, whereas for sandstone, the matrix porosity is considerable. Table 2.1 shows that there is a large difference between the total n and the effective porosity n_e. The total porosity includes all the pores of the system whereas, for the effective porosity, only connected pores that are available to fluid flow are considered. It is important to point out that the effective porosity is not directly correlated with the hydraulic conductivity of the system. The hydraulic conductivity varies over a wide range for different rock types as well as for one single rock type.

This book is concerned with *fractured porous rock*, in which the rock matrix is considered to be permeable to flow. Fractured porous rock is generally divided into three different components:

- A *fracture network* is a system of partially intersecting single fractures. Its hydraulic properties are typically characterized by the distribution of fracture size, fracture permeability, fracture orientation, fracture distance, and fracture density. Due to its small volume relative to the volume of the total domain, the storage capacity of the fracture system is small.
- Within the fractures, *filling material* consisting of mineral deposits can be found. Open fractures can channel and speed up the transport of pollutants from disposal sites, e.g. leading to a locally high concentration of a

Table 2.1. Total porosity, effective porosity and hydraulic conductivity of selected hard rocks (Domenico and Schwartz (1990); Matthess and Ubell (1983)).

Rock	Total porosity n (%)	Effective porosity n_e (%)	Hydraulic conductivity K ($m\,s^{-1}$)
Granite	0.1	0.0005	$0.5 \cdot 10^{-12} - 2.0 \cdot 10^{-12}$
Limestone	5 – 15	0.10 – 5	$1.0 \cdot 10^{-09} - 6.0 \cdot 10^{-06}$
Chalk	5 – 44	0.05 – 2	$6.0 \cdot 10^{-09} - 1.4 \cdot 10^{-07}$
Sandstone	5 – 20	0.5 – 10	$3.0 \cdot 10^{-10} - 6.0 \cdot 10^{-06}$
Shale	1 – 10	0.5 – 5	$1.0 \cdot 10^{-13} - 2.0 \cdot 10^{-09}$

pollutant at a great distance from the source, whereas filled fractures may inhibit the flow in otherwise highly permeable aquifers (Odling, 1995).

- The *matrix* blocks between the fractures have a spatially varying texture and porosity. The permeability contrast between fractures and matrix is decisive for the importance of the matrix for flow and transport processes. As opposed to the fracture system, the storage capacity of the matrix is often significant as a result of its large volume relative to the total domain.

The research results discussed in this book are obtained from flow and transport experiments in fractured porous systems on different scales. This means that the matrix is permeable to flow and plays a significant role for both flow and transport within the experimental domains. Open as well as filled fractures occur, in most cases acting as preferential flow paths. In some cases, however, the filling material inhibits the flow.

In order to characterize a fractured system, criteria and properties must be defined that can be qualitatively or quantitatively determined directly in the field or in laboratory investigations. Since the evaluation of fracture geometry and the generation of fracture systems for modeling are discussed in this book, some frequently used properties are now briefly presented.

Fracture Size

The fracture size, i.e. the lateral limitations of a fracture, can in most cases not be recorded and determined directly. Usually, fracture traces are detected at exposed walls (e.g. outcrops, quarries, tunnels). The fracture trace is the intersection line of a fracture with the exposed wall. In the field, the actual fracture sides are therefore often not determined, but the fracture traces are recorded and evaluated further using statistical methods. These difficulties are demonstrated in Fig. 2.3. The vertical two-dimensional section, showing the fracture intersection lines with the x-y-plane at $y = 1\,m$, is only a limited representation of the actual three-dimensional system.

The approximation of the empirical fracture trace length distribution can be accomplished using different theoretical distribution functions, e.g. power

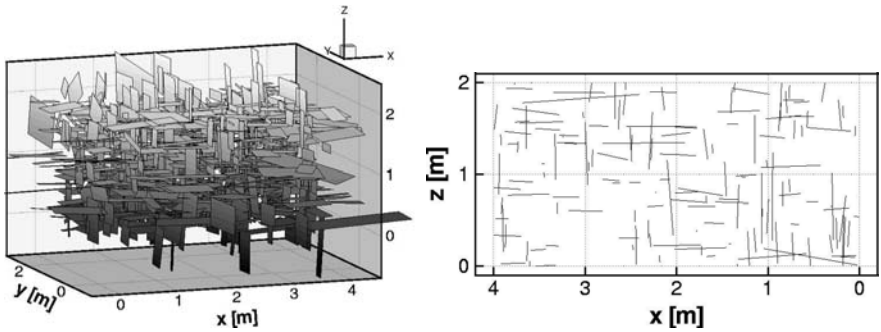

Fig. 2.3. Artificial three-dimensional fracture system (left) and a vertical two-dimensional section showing the fracture traces at $y = 1$ m (right).

law, log-normal, hyperbolic or gamma-1 distributions. References for these distributions are given by Dershowitz and Einstein (1988). They explain the diversity of possible distributions by the fact that fracture traces and not the actual fracture sides are detected, and by the processes that cause the formation of fractures. An interesting aspect is whether it is possible to reconstruct the actual three-dimensional fracture system based on the determined fracture-trace distribution. Considering fractures with circular shape, Baecher *et al.* (1977) show that a power law and a log-normal distribution of the fracture radii both lead to a log-normal distribution of the fracture traces. Hence, a unique reconstruction of the fracture system is not possible.

Fracture Distance

The fracture distance is defined as the distance measured between two directly neighboring fractures along a straight line. The fracture distance, or the distribution of the fractures distance controls the geometrical arrangement of the fractures. According to Meier and Kronberg (1989), the principle of the fracture distance is based on the idea that the formation of a fracture causes a tension decrease in the vicinity of the fracture. The next fracture can only be formed if the critical regional tension occurs again, causing the genesis of another fracture. In sedimentary rock, the fracture distance depends, for example, on the elastic properties of the individual layers of a sedimentary sequence, the thickness of the layers, the permeabilities and the deformation intensity.

According to Priest (1993), three different definitions of fracture spacing can be distinguished:

- *Total spacing*: Distance between two directly neighboring fractures with different orientation measured along a straight line.
- *Set spacing*: Distance between two directly neighboring fractures with equal orientation measured along a straight line.

- *Normal set spacing:* Distance between two directly neighboring fractures with equal orientation measured along a straight line that is parallel to the mean normal direction of the fractures.

Extensive field investigations have shown that a POISSON distribution, describing the arrangement of the fractures in space, corresponds to a power-law distribution of the fracture distances. Sachs (1997) circumscribes the POISSON distribution as follows: "The POISSON distribution is valid, if the average number of events is the result of a large number of event possibilities and a very small event probability. The POISSON distribution is used to solve problems that occur when counting relatively rare random and independent events in time, length, area or space domains".

The determination of the fracture distance is schematically represented in Fig. 2.4.

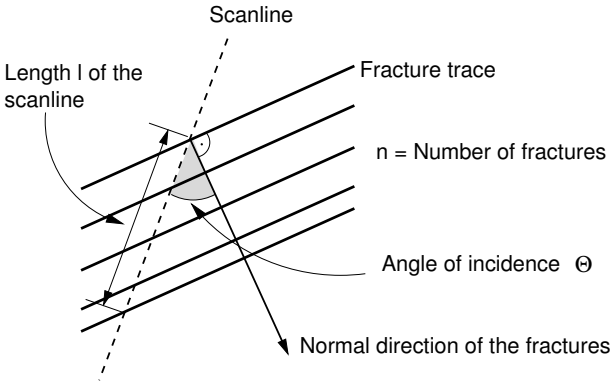

Fig. 2.4. Determination of fracture distances.

The mean fracture distance can be determined from the length l of the scanline, the number of fractures n and the angle of incidence θ between the scanline and the normal direction of the fractures:

$$\text{mean distance} = \frac{l}{n} \cdot \cos\theta \,. \tag{2.1}$$

Fracture Density

The fracture density is determined on the basis of core samples and scanline measurements. Scanlines are observation lines, positioned on an exposed wall. Along the scanline, the number of intersections with fractures, the angle of incidence etc. can be determined.

The one- and two-dimensional fracture density d_1 and d_2 (see below) are, except for isotropic systems, dependent on the orientation of the scanline and

the exposed wall. The volumetric fracture density d_3, i.e. the mean fracture area per unit volume, is, according to Chilès and de Marsily (1993), determined by:

$$d_3 = \frac{1}{l} \sum_{i=1}^{n} \frac{1}{\sin \theta_i}, \tag{2.2}$$

where θ_i is the angle of incidence of the fracture, l is the length of the scanline and n is the number of fractures per scanline.

For randomly distributed fracture orientations, the following two relationships between the volumetric fracture density d_3 and the linear fracture density d_1 and the area-related fracture density d_2, respectively, are obtained. The linear fracture density d_1 describes the average number of fractures per unit length along a line:

$$d_1 = \frac{1}{2} d_3 . \tag{2.3}$$

The area-related fracture density d_2 defines the average fracture length per unit area:

$$d_2 = \frac{\pi}{4} d_3 . \tag{2.4}$$

Fracture Aperture

The fracture aperture is defined as the perpendicular distance between two directly neighboring fracture walls. The aperture can be increased by, for example, dissolution and erosion processes. This is mainly observed in the weathered zones close to the ground surface. Another reason for an increase in aperture is displacement due to external forces or subsidence. The aperture generally decreases with increasing depth due to the increasing thickness of the overlying rock.

Figure 2.5 shows two sides of a fracture. The roughness of the two surfaces can be clearly seen. If the two pieces are put together, the actual fracture is obtained as the space between the two surfaces. The aperture varies significantly throughout a fracture. It is therefore not possible to characterize the fracture aperture by a single measurement. In the case of single fractures, one possibility is to assume a heterogeneous fracture-aperture distribution; however, for the consideration of multiple fractures or fracture systems, this approach is made impossible by the degree of detail required.

In general, for the discrete representation of fractures in models, the fracture aperture is described using the parallel-plate concept. This concept is explained in detail in Sect. 2.4.1.

The fracture aperture has an essential influence on the flow and transport processes in a fractured system. However, the determination of the aperture is not trivial (Chilès and de Marsily, 1993):

- In nature, there is no constant aperture throughout a fracture plane. There are closed and open regions.

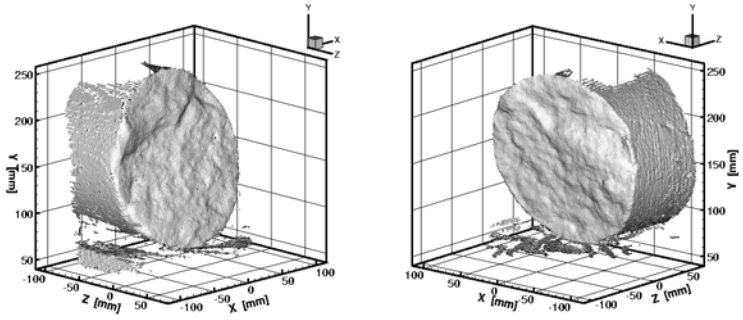

Fig. 2.5. Image of the two opposite walls of a single fracture from a sandstone core sample with a diameter of approximately 20 cm (created in cooperation with the Institute for Robotics and Process Control, Technical University of Braunschweig, Germany).

- The flow between two parallel plates (parallel-plate concept), separated by a constant aperture, has little in common with the actual flow through a natural fracture.
- Due to the pressure release that a sample experiences during sample extraction, the measured aperture deviates from the aperture that would be measured *in situ*.

Fracture Orientation

The orientation of geological formations in space is uniquely determined by the strike angle S_t or the azimuth A_z, and the dip D_i. According to Murawski (1998), the strike is the section boundary of a natural surface (e.g. layer or fracture) at an imaginary horizontal plane. The strike angle S_t is defined as the angle between the northerly direction and the section boundary. The projection of the line of greatest slope onto the horizontal plane is the dip direction and is always perpendicular to the strike. The inclination angle between the line of greatest slope and the dip direction is the dip D_i. The angle between the northerly direction and the dip direction is defined as the azimuth A_z. It is connected to the strike angle through the equation $A_z = S_t + 90°$. Figure 2.6 summarizes the relationship between strike, dip and azimuth.

If fractures or layers occur in a preferred direction, the statistical distribution of the orientation is often described by the FISHER distribution, also called the spherical normal distribution. The FISHER distribution is characterized by the fact that orientations are distributed around a certain main orientation with rotational symmetry. In Wallbrecher (1986) and Fisher *et al.* (1993), the distribution is discussed in detail. The probability density function of the FISHER distribution has the following form:

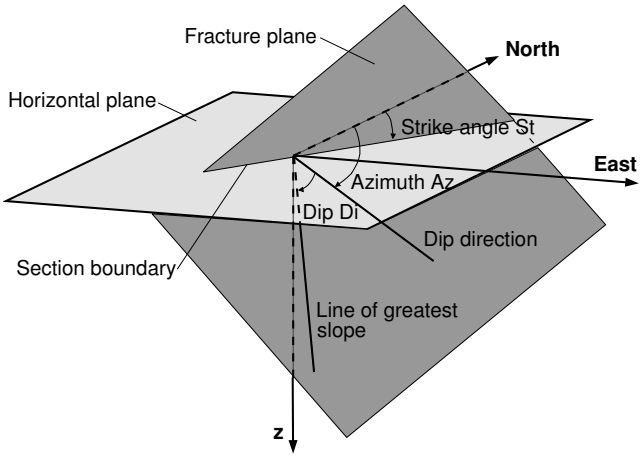

Fig. 2.6. Determination of the location of a geological surface: strike, dip, azimuth. The dip direction is the projection of the line of greatest slope onto the horizontal plane.

$$f(\Theta,\phi) \;=\; \frac{\kappa}{4\pi\cdot\sinh\kappa}\cdot exp[\kappa\,(\sin\Theta\;\sin\alpha\;\cos(\phi-\beta) \;+\; \cos\Theta\;\cos\alpha)]\cdot\sin\Theta\;. \tag{2.5}$$

Here, α is the Θ-pole coordinate (latitude) of the main direction, β is the ϕ-pole coordinate (longitude) of the main direction and κ is the concentration parameter. The concentration parameter κ is a measure of the distribution of the orientations around the main orientation. For $\kappa = 0$, the orientations are uniformly distributed. The larger κ is, the stronger the concentration around the main orientation. The *cone of confidence* is used to quantify the significance of the distribution. The cone of confidence yields a small circle around the main orientation R_i. The calculation of the cone of confidence is only permissible for $\kappa \geq 4$. For $\kappa < 4$, there is no spherical normal distribution or the sample size is too small. The measures for the cone of confidence are the spherical variance

$$S^* \;=\; \frac{n-|R_i|}{n} \tag{2.6}$$

and the spherical aperture

$$\omega = \arcsin\sqrt{2\frac{1-1/n}{\kappa}}\;. \tag{2.7}$$

Here, R_i is the main orientation and n is the sample size. Figure 2.7 shows the relationship between the main direction R_i and the spherical aperture ω. The spherical aperture for the FISHER distribution corresponds to the standard deviation of the GAUSSIAN normal distribution.

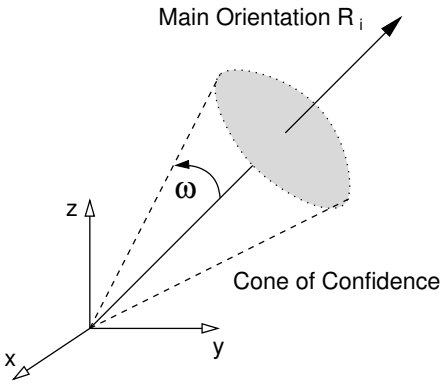

Fig. 2.7. Sketch of the cone of confidence with the spherical aperture ω.

Orientation data are represented graphically in pole diagrams. The intersection points of the normal vectors of the planes with one half of a globe are projected onto a circular area. Examples of such diagrams are shown and discussed in Sect. 5.3.

2.2 Model Concepts in Fractured Porous Systems

M. Süß, R. Helmig

As discussed in the introduction to this chapter, it is not possible to set up a model that is an exact representation of reality, but conceptual models are developed that are able to describe the relevant structures and physical processes of a problem. The choice of a model concept for the description of fractured media strongly depends on the scale of the problem, the geological characteristics of the area of investigation, and the purpose of the simulation. Bear (1993) classifies various problems of flow and transport in fractured porous media according to their scale. On these scales, different types and extensions of heterogeneities occur (Rats and Chernyashov, 1967).

- **Zone 1: The very near field.** Interest is focused on flow and transport processes within small-scale fractures (fissures) and the pore space. Single, well-defined fractures and the surrounding porous rock, which is possibly accessible to transport, are considered.
- **Zone 2: The near field.** The flow and transport processes are considered in a relatively small domain, which contains a small number of well-defined small and intermediate fractures. The location and shape of the individual fractures are either deterministically defined or can be generated stochastically, based on statistical information from the real system.
- **Zone 3: The far field.** On this scale, the flow and transport processes are regarded as taking place, simultaneously, in at least two continua. One

continuum is composed by the network of large scale fractures and the other one by the porous rock. Mass of the fluid phase and its components may be exchanged between the two continua.

- **Zone 4: The very far field.** The entire fractured medium is considered as one single continuum, possibly heterogeneous and anisotropic in order to account for large scale geological layers and fault zones.

In order to set up models of systems with such varying characteristics, different model concepts are necessary. These concepts are discussed on the basis of Fig. 2.8. Two principal approaches are possible (Helmig, 1993):

1. Assuming that the concept of the *representative elementary volume* (REV) (see Sect. 2.3.1) is valid and that the scale of the investigation area is sufficiently large, it is possible to describe the model area as a heterogeneous, anisotropic *continuum*. According to Bear (1993), this is possible on the very far scale. Kröhn (1991) also considers this to be a feasible approach for describing poorly fractured rock (type I) and rock with a very high fracture density (type II) on a smaller scale.
2. If the flow and transport processes in the fractured media are dominated by shear zones (spatially concentrated small-scale fractures) or fracture systems, it is feasible to describe these features specifically, neglecting the rock matrix, using a *discrete* fracture network model (consideration of each single fracture) (type III).

However, the rock matrix, filling the space between the fractures, is often not negligible, but plays an essential role in flow and transport processes. If the porous rock matrix can be idealized as a continuum with averaged material properties, a model can be set up where a continuum model, accounting for the matrix, is coupled with a discrete model considering the fractures (Fig. 2.8, type IV). This type of model is further discussed in Sect. 2.4.

Another widely used possibility for describing areas of type II (system with high fracture density) and IV (dominant single fractures + rock matrix) (Fig. 2.8) is to transform the matrix and the fracture systems on different scales into separate homogeneous equivalent continua. This approach is mainly applied on large scales. With the concept originally presented by Barenblatt *et al.* (1960), the flow and the transport processes between the continua can be represented by coupling them via exchange terms and in this way setting up a so-called double-continuum model. It is essential to the principle of homogenization for heterogeneous media to define equivalent model parameters and to find appropriate expressions for the interaction of the hydraulic components which are capable of describing the correct physical system behavior. Extending this model allows the consideration of more than two continua, a multi-continuum model, if required by the geological characteristics of the investigation area and by the nature of the problem. This type of model concept is further described in Sect. 2.5.

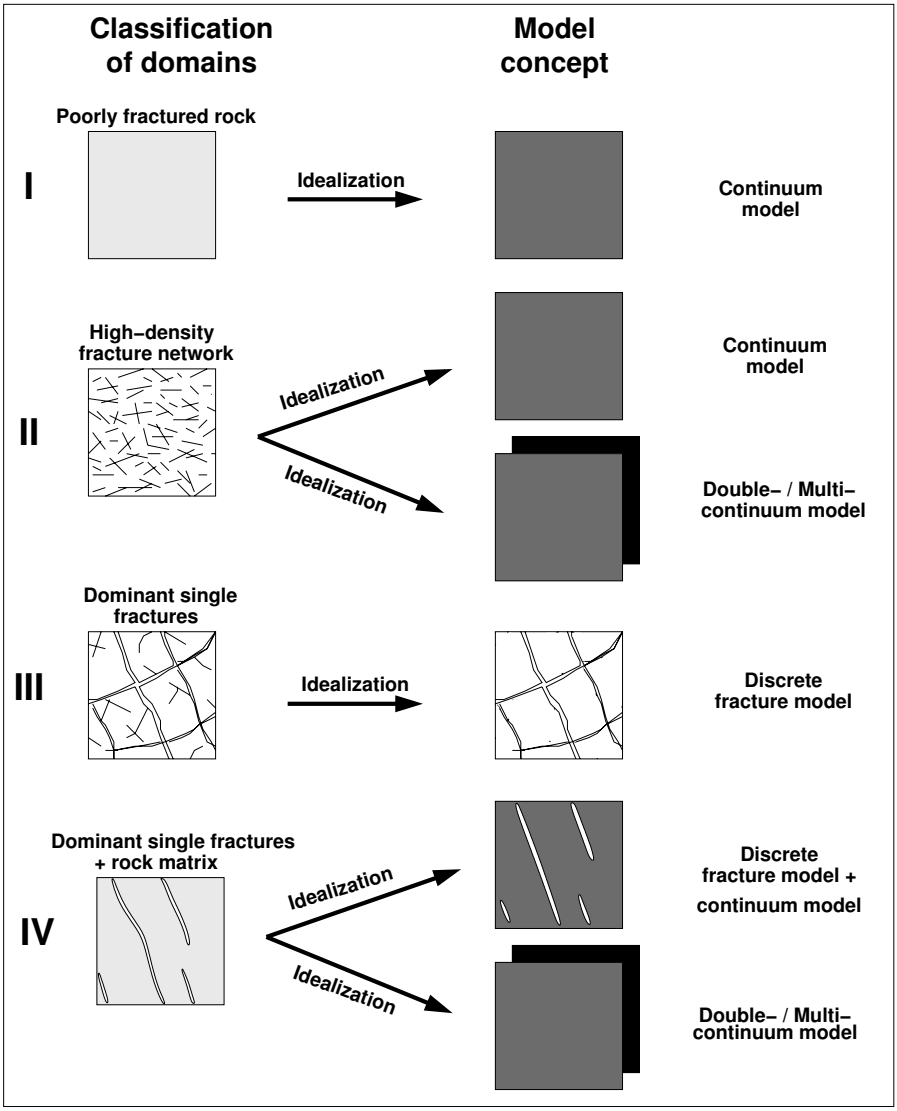

Fig. 2.8. Model concepts for the description of fractured porous media (based on Kröhn (1991) and Helmig (1993)).

2.3 Governing Equations of Flow and Transport in Porous Media

M. Süß, A. Silberhorn-Hemminger, R. Helmig

In this section, the mathematical description and the governing equations of flow and transport processes in *porous media in general*, i.e. without the con-

sideration of fractures, are presented. The discussion focuses on the processes which are relevant to the research work presented in this book. The implementation of the discrete and the multi-continuum concepts for considering the fractures is discussed in Sects. 2.4 and 2.5 respectively.

2.3.1 Representative Elementary Volume

The concept of the *representative elementary volume* (REV) as defined by Bear (1972) is fundamental to the mathematical description of fluid flow and transport in porous media. By means of volume averaging, the micro-scale properties of the porous medium (grain-size and pore-space geometry) are represented by an equivalent continuum on a larger scale described by new properties. On the one hand, the REV must be large enough to avoid undesirable fluctuations of the averaged properties, and on the other hand, it must be small enough to render the spatial dependency of these properties. In Fig. 2.9, the definition of a suitable extent of the REV is visualized. The application of the REV approach in different model concepts for *fractured* porous media is discussed in Sects. 2.2, 2.4 and 2.5.

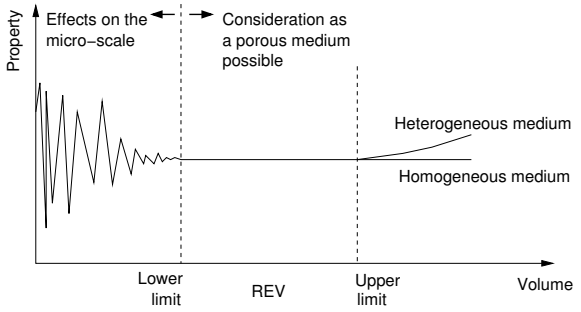

Fig. 2.9. Representative elementary volume (REV) (modified from Bear (1972)).

2.3.2 Flow Processes

2.3.2.1 DARCY Equation

The DARCY equation for laminar flow in porous media was defined by HENRY DARCY in 1856. In one-dimensional column experiments, DARCY found that the volume discharge Q is proportional to the hydraulic gradient $\Delta h/\Delta l$ as described by the following equation:

$$Q = -A\,K\,\frac{\Delta h}{\Delta l}\,. \tag{2.8}$$

Here, A is the cross-sectional area of the column, K is the hydraulic conductivity, Δh is the difference in hydraulic head and Δl is the distance between the measurement points. From (2.8) and the relationship

$$Q = q_i A , \tag{2.9}$$

the three-dimensional DARCY velocity q_i is determined:

$$q_i = -K_{ij} \frac{\partial h}{\partial x_j} . \tag{2.10}$$

The hydraulic conductivity tensor K_{ij} depends on the properties of the porous medium as well as of the fluid:

$$K_{ij} = \frac{\rho \, g \, k_{ij}}{\mu} , \tag{2.11}$$

where ρ is the fluid density, g is the gravitational acceleration, k_{ij} is the permeability tensor and μ is the dynamic viscosity. The permeability tensor k_{ij} represents the directional resistance of a porous medium and is independent of the fluid properties. Expressing the piezometric head h as a pressure p and inserting the permeability k_{ij} instead of the hydraulic conductivity K_{ij}, yields the following expression for the DARCY velocity q_i:

$$q_i = -\frac{k_{ij}}{\mu} \left(\frac{\partial p}{\partial x_j} + \rho g \frac{\partial z}{\partial x_{ij}} \right) . \tag{2.12}$$

In the case of gas flow, the gravity effect is often neglected. This is legitimate if the gravity effect, due to low density, is small compared to the effect of the pressure gradient. Neglecting the gravity effect, the equation can be simplified to

$$q_i = -\frac{k_{ij}}{\mu} \frac{\partial p}{\partial x_{ij}} . \tag{2.13}$$

This form of the equation may be applied for two-dimensional horizontal calculations as well.

The range of validity of the DARCY equation is expressed in terms of the REYNOLDS number Re. According to Bear (1972), the upper limit of the validity of the DARCY equation is at a value of Re between 1 and 10.

2.3.2.2 Continuity Equation

The continuity equation is based on the principle of conservation of mass, and states that the temporal change of mass in a control volume is the sum of the mass flux across the volume boundaries and the mass flux due to sources and sinks. The temporal change of the mass in the control volume is described as follows:

$$\frac{\partial(n\rho)}{\partial t} = -\frac{\partial(\rho q_i)}{\partial x_i} + q_\mathrm{s} \; . \tag{2.14}$$

Here, q_s is the source and sink term, e.g. describing well withdrawal or injection, and n represents the total porosity, also including the pores through which there is no flow. The porosity is slightly pressure-dependent (Kinzelbach, 1992). However, this aspect is neglected here, i.e. the matrix is considered as inelastic. From this, the continuity equation is obtained in the following form:

$$n\,\frac{\partial \rho}{\partial t} = -\frac{\partial(\rho q_i)}{\partial x_i} + q_s \; . \tag{2.15}$$

If we introduce the piezometric head h as the independent variable instead of the DARCY velocity q_i, we may express the continuity equation as

$$n\,\frac{\partial \rho}{\partial t} = \frac{\partial}{\partial x_i}\left(\rho^2 g\,\frac{k_{ij}}{\mu}\,\frac{\partial h}{\partial x_i}\right) \; . \tag{2.16}$$

The source and sink term q_s is omitted for simplicity's sake. This general expression is valid for heterogeneous, anisotropic and compressible media. Bear (1972) rewrites (2.16) for the independent variable pressure p using the relationship

$$g\,\frac{\partial h}{\partial x_i} = g e_{x_3} z + \frac{1}{\rho}\,\frac{\partial p}{\partial x_i} \; , \tag{2.17}$$

where e_{x_3} is the unit vector in z-direction. Assuming that $k_{ij} = 0$ for $i \neq j$, this results in the expression

$$n\frac{\partial \rho}{\partial t} = \frac{\partial}{\partial x_1}\left(\rho\frac{k_1}{\mu}\frac{\partial p}{\partial x_1}\right) + \frac{\partial}{\partial x_2}\left(\rho\frac{k_2}{\mu}\frac{\partial p}{\partial x_2}\right) + \frac{\partial}{\partial x_3}\left(\rho\frac{k_3}{\mu}\left[\frac{\partial p}{\partial x_3} + \rho g\right]\right) . \tag{2.18}$$

In (2.18), the term ρg, expresses the gravity effect. In many cases, this effect is much smaller than the pressure gradient $\partial p/\partial x_3$, and is therefore neglected (Bear, 1972).

Depending on the fluid, the pressure dependency of the fluid density ρ is more or less significant, e.g. water is generally assumed to be incompressible whereas gas is highly compressible. The experiments and the numerical simulations discussed in this book are mainly concerned with gas-saturated media. Assuming an ideal gas, the relationship between the density and the pressure is described by the ideal gas law:

$$\rho = \frac{p}{R_\mathrm{i} T} \; . \tag{2.19}$$

Here, R_i is the individual gas constant and T is the temperature.

Introducing (2.19) into (2.18) and neglecting the gravity term, the following diction of the continuity equation is obtained:

$$n\,\frac{\partial p}{\partial t} = \frac{\partial}{\partial x_i}\left(\frac{k_{ij}}{2\mu}\,\frac{\partial p^2}{\partial x_i}\right) \; . \tag{2.20}$$

2.3.3 Transport Processes

Assuming a conservative tracer, i.e. no adsorption and no reactions, in an isothermal system, three mechanisms determine the transport process, namely advection, dispersion and diffusion.

2.3.3.1 Advection

Advective transport comprises the movement of the tracer in the direction and with the average fluid velocity of a control volume (Kinzelbach, 1992). Here, the determining velocity is the seepage velocity v_i defined as:

$$v_i = \frac{q_i}{n_\mathrm{e}} \,. \tag{2.21}$$

Dividing by the effective porosity n_e, and not by the total porosity n, takes into account that the fluid can only flow through the connected pore space of the control volume, i.e. not through the dead-end pores. The seepage velocity v_i is a bulk property and is therefore only indirectly measurable. The advective mass flux is expressed as

$$J_{\mathrm{a},i} = c v_i \,, \tag{2.22}$$

where c is the solute concentration of the transported substance.

2.3.3.2 Hydrodynamic Dispersion

Dispersion describes the mixing of two miscible fluids due to fluctuations around the average velocity, caused by the morphology of the medium, the fluid flow condition and chemical or physical interaction with the solid surface of the medium (Sahimi, 1995). The concept generally used to describe this mixing process is based on FICK's law, assuming that there is a compensation of the concentration in the direction of the negative concentration gradient. The dispersive mass flux is expressed as

$$J_{\mathrm{d},i} = - D_{\mathrm{d},ij} \frac{\partial c}{\partial x_j} \,, \tag{2.23}$$

where $D_{\mathrm{d},ij}$ is the dispersion tensor. Dispersive mixing is assumed to take place in two principal directions, longitudinal and transversal to the direction of the seepage-velocity vector v_i. The dispersion tensor $D_{\mathrm{d},ij}$ is not constant, but depends on the seepage-velocity v_i. Provided that the system of coordinates is aligned with the direction of flow, the dispersion tensor $D_{\mathrm{d},ij}$ is diagonal:

$$D_{\mathrm{d},ij} = \begin{bmatrix} D_\mathrm{l} & 0 & 0 \\ 0 & D_\mathrm{t} & 0 \\ 0 & 0 & D_\mathrm{t} \end{bmatrix} = \begin{bmatrix} \alpha_\mathrm{l} v_1 & 0 & 0 \\ 0 & \alpha_\mathrm{t} v_2 & 0 \\ 0 & 0 & \alpha_\mathrm{t} v_3 \end{bmatrix} \,. \tag{2.24}$$

Here, D_l and D_t are the longitudinal and the transversal dispersion coefficients respectively, assuming that the vertical and the horizontal transversal dispersivity is equal. α_l and α_t are the longitudinal and the transversal dispersion lengths. The ratio between α_l and α_t is generally larger than 1.

Diffusion induces a mass flux between regions of different concentration. Mass flux occurs in the direction of the negative concentration gradient and is described by FICK's law:

$$J_{\mathrm{m,e},i} \;=\; -\, D_\mathrm{m,e}\, \frac{\partial c}{\partial x_i}\,. \tag{2.25}$$

Here, $D_\mathrm{m,e}$ is the effective diffusion coefficient which takes into account that the diffusion process is dependent not only on the combination of fluids, on the temperature and the pressure (Reid *et al.*, 1987) but also on the porous medium (Grathwohl, 1998). The diffusion coefficient for gases is higher than for liquids. Since the diffusion process is slow, the significance of this mass flux depends on its relative importance compared to the advective and the dispersive fluxes. In regions of high velocities, it may be neglected, whereas for low velocities, it is one of the essential processes that determine the shape of the tracer-breakthrough curve. Since, in this book, first, most of the cases discussed involve gas flow and, second, the investigations are concerned with flow in fractured low-permeable porous media, the diffusive processes may not be neglected.

From the above discussion, it is obvious that dispersive as well as diffusive processes are implemented according to the same concept, i.e. FICK's law. Consequently, these transport flux terms may be combined in one term, generally defined as the *hydrodynamic-dispersion* term, where $D_{\mathrm{d},ij}$ and $D_\mathrm{m,e}$ are summarized in the hydrodynamic-dispersion tensor D_{ij} (Scheidegger, 1961):

$$D_{ij} = \begin{bmatrix} D_\mathrm{m,e} + \alpha_\mathrm{l} v_1 & 0 & 0 \\ 0 & D_\mathrm{m,e} + \alpha_\mathrm{t} v_2 & 0 \\ 0 & 0 & D_\mathrm{m,e} + \alpha_\mathrm{t} v_3 \end{bmatrix}. \tag{2.26}$$

The mass flux due to hydrodynamic dispersion is expressed by:

$$J_{\mathrm{hd},i} \;=\; -\, D_{ij}\, \frac{\partial c}{\partial x_j}\,. \tag{2.27}$$

The concept of hydrodynamic dispersion accounts for the spreading of the tracer due to the irregular pore space. On a larger scale, the concept of *macro-dispersion* accounts for dispersion due to heterogeneities of the porous medium. In continuum models, a FICKIAN approach is often chosen for the macro-dispersion. In, for example, Cirpka (1997), the concept of macro-dispersion as well as different model approaches are discussed in detail.

2.3.3.3 Transport Equation

Following the same principle as for the continuity equation (2.14), the transport equation is derived by balancing all mass fluxes across the boundaries of a control volume:

$$J_i + \frac{\partial}{\partial x_i}\left(J_{\mathrm{a},i} + J_{\mathrm{hd},i}\right) = 0\,. \tag{2.28}$$

If J_i is expressed as

$$J_i = \frac{\partial c}{\partial t} + q_{\mathrm{m}}\,, \tag{2.29}$$

where q_{m} is the tracer mass source/sink term, (2.28) can be written as

$$\frac{\partial c}{\partial t} + \frac{\partial}{\partial x_i}(v_i c) - \frac{\partial}{\partial x_i}\left(D_{ij}\frac{\partial c}{\partial x_j}\right) + q_{\mathrm{m}} = 0\,. \tag{2.30}$$

A measure of the relative importance of advective and dispersive/diffusive transport is the PECLET number Pe. It is defined as

$$Pe = \frac{|v|\,L}{|D_l|}\,, \tag{2.31}$$

where v is the average seepage velocity in flow direction, L is a typical length scale of the problem and D_l is the hydrodynamic dispersion coefficient in the flow direction. Large PECLET numbers indicate that advection dominates the transport process.

2.4 The Discrete Model Concept

A. Silberhorn-Hemminger, M. Süß, R. Helmig

As discussed above, in situations where the fractures as well as the matrix play a significant role for the flow and transport processes, the model domain cannot be homogenized but a model concept that includes fractures as well as matrix is required. One approach is to use the discrete model concept, where the matrix and the fractures are locally idealized as continua and the fractures are implemented discretely at their actual location within the domain. It is obvious that the amount of data required to set up a discrete model of the actual domain is very large and to some extent not measurable. Consequently, the discrete model concept is preferably used for relatively small domains and is a suitable tool for principle studies of flow and transport processes.

In the previous sections (2.3), the physical-mathematical description of the flow and transport processes in porous media, i.e. in the porous matrix,

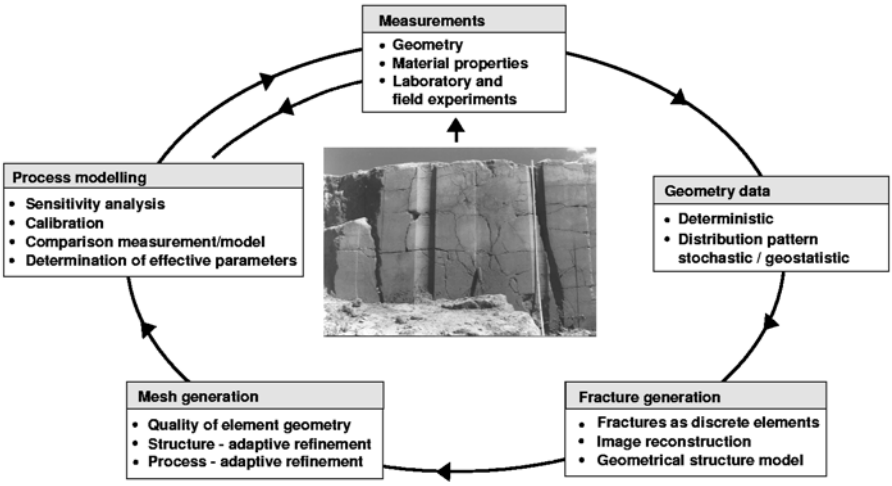

Fig. 2.10. Discrete modeling of flow and transport processes in fractured porous media - necessary steps.

is presented. This section deals with the model concept specific to the fractures and the mathematical description of the flow within a fracture as well as of its location and geometry. The stochastic fracture generator FRAC3D is presented and the implementation of the discrete model concept in the numerical model is briefly discussed. Figure 2.10 shows the steps from a natural system to a discrete process model.

2.4.1 Parallel-Plate Concept

A natural fracture is bounded on both sides by the rock surface (Fig. 2.5). The rough fracture walls do not have an identical profile and the normal tension is carried by contact zones between the walls. A model concept frequently used for a fracture consists of two plane parallel plates, representing the fracture walls. As illustrated in Fig. 2.11, it can be applied locally, maintaining a variation in fracture aperture throughout the fracture, or globally, assuming one constant aperture for the total fracture. It is a well-known fact that especially the latter approach is a strong simplification of nature. However, other methods proposed in the literature have not yet found general acceptance (Berkowitz, 2002).

Tsang and Tsang (1987) showed that preferential flow paths exist, hence *channeling* effects may have significant influence on the flow and therefore also on the transport processes. For multi-phase flow, the variation in entry pressure is strongly related to the distribution of the aperture; therefore channeling effects are particularly important for simulations including more than one fluid phase.

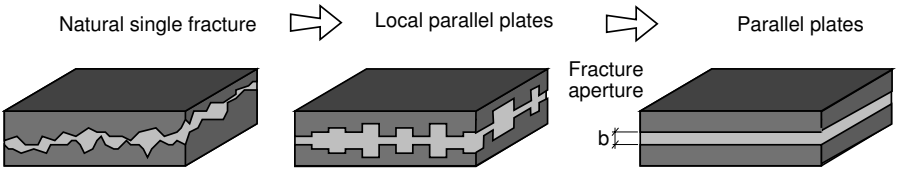

Fig. 2.11. From nature to parallel-plate concept.

For the numerical studies presented in this book, the parallel-plate concept is applied. The decision to use this simplified concept is justified by the fact that the simulations are concerned with single-phase flow only and that, for the principle character of the investigations, this approximation of nature is sufficient.

When the parallel-plate concept is applied, it is assumed that the length scale l of the plates is much larger than the distance between them b ($l \gg b$). Furthermore, hydraulically smooth walls and laminar flow are assumed, corresponding to the POISEUILLE fluid model (Wollrath, 1990) . Figure 2.12 shows the two parallel plates and the parabola-shaped velocity profile, indicating laminar flow. The NAVIER-STOKES equation for the laminar single-

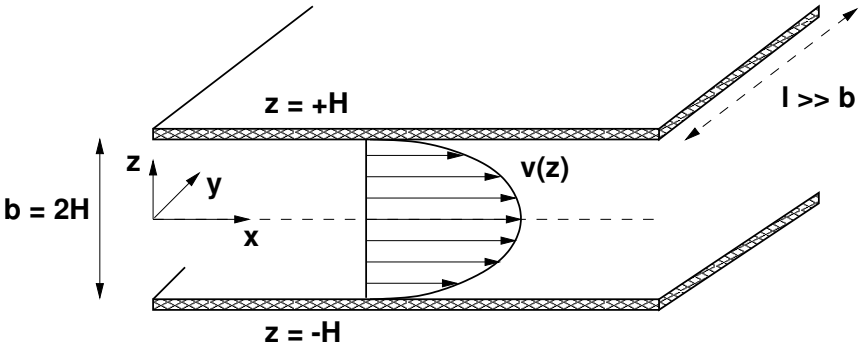

Fig. 2.12. Laminar flow between two parallel plates: parabola-shaped velocity profile.

phase flow of an incompressible NEWTONIAN fluid yields the following equation for the velocity profile between two parallel plates (Snow (1969); White (1999)):

$$v(z) \;=\; \frac{\rho g}{2\mu}\left[-\frac{d}{dx}\left(\frac{p}{\rho g} \;+\; z\right)\right]\left(H^2 \;-\; z^2\right). \tag{2.32}$$

The maximum velocity $v_{\max}$ is reached at $z = 0$:

$$v_{\max} \;=\; v(z=0) \;=\; \frac{\rho g}{2\mu}\, H^2 \;\cdot -\, \frac{d}{dx}\left(\frac{p}{\rho g}\right). \tag{2.33}$$

For a parabola-shaped profile, the mean velocity $\overline{v}$ is derived from the maximum velocity $v_{\max}$:

$$\overline{v} \;=\; \frac{2}{3}\, v_{\max} \;=\; \frac{\rho g}{\mu}\,\frac{H^2}{3}\;\cdot -\,\frac{d}{dx}\left(\frac{p}{\rho g}\right)\;. \tag{2.34}$$

From (2.34) and under consideration of the distance between the plates b ($b = 2H$), the mean three-dimensional velocity $\overline{v}_i$ can be written as:

$$\overline{v}_i \;=\; -\,\frac{b^2}{12}\,\frac{\rho g}{\mu}\,\frac{\partial h}{\partial x_i} \;=\; -\,K\,\frac{\partial h}{\partial x_i}\;. \tag{2.35}$$

Here, the hydraulic conductivity K and the permeability k have the following relationship (see (2.11)):

$$K \;=\; k\,\frac{\rho g}{\mu} \qquad\qquad \text{with} \qquad\qquad k \;=\; \frac{b^2}{12}\;. \tag{2.36}$$

From this, it can be concluded that the permeability of a fracture, approximated by the parallel plate concept, is proportional to the square of the fracture aperture b. The volume discharge Q is derived by integrating the velocity over the distance between the plates (assuming a constant depth l parallel to the y-axis):

$$Q \;=\; \int_{-H}^{+H} v(z)\; l\; dz\;. \tag{2.37}$$

Including (2.32) yields:

$$Q \;=\; -\,\frac{\rho g}{\mu}\,\frac{b^3}{12}\; l\;\frac{\partial h}{\partial x_1} \tag{2.38}$$

Due to the proportionality of Q to the third power of the aperture b, (2.38) is referred to as the *cubic law* (Romm, 1966).

2.4.2 Generation of Fracture Structural Models – FRAC3D

The use of the discrete modeling approach for simulating flow and transport processes in fractured porous media requires the discrete description of the fractures in space. Here, the fracture generator provides the geometrical description and the structural properties of the fracture system. The fracture generator represents a link between the natural and the numerical model.

The generating algorithm requires information on the geometrical characteristics of the fractures. This is obtained by investigating core samples or outcrop sites. The information gained from these samples and locations is of one- or two-dimensional character. Here, one problem of generating a

stochastic fracture field, particularly a three-dimensional fracture field, becomes obvious: the information content of the data does not account for the clearly three-dimensional characteristics of fractured porous systems. The reliability of such stochastically generated geometric models depends strongly on the qualitative and quantitative description of the aquifer system: are there main fracture orientations, is the fracture density high or low, is there a single dominating fracture or fault zone, are the fractures open, are they filled, how wide and rough are the fractures? These questions are just a selection of many more that have to be answered or at least to be considered during the process of generating stochastic fracture systems. Additionally, we assume that the selected real aquifer from which the field data is obtained can be considered representative of the ensemble of all possible realizations. The stochastic properties of the ensemble are given by adapted theoretical distributions. Consequently, a stochastically generated fracture network based on the field data can be regarded as one possible realization out of the ensemble. The fracture-generating algorithm makes it possible to combine the available field information adequately in order to obtain structural geometric fracture models which are realizations of the real aquifer system.

In structural models, the natural fractures are represented by discrete elements. In a two-dimensional model, the fractures are one-dimensional elements. In a three-dimensional model, the fracture planes are two-dimensional elements. Additionally, distinctive flow channels may be represented by one-dimensional elements in the three-dimensional model. Figure 2.13 shows a two- and a three-dimensional stochastic structural fracture model.

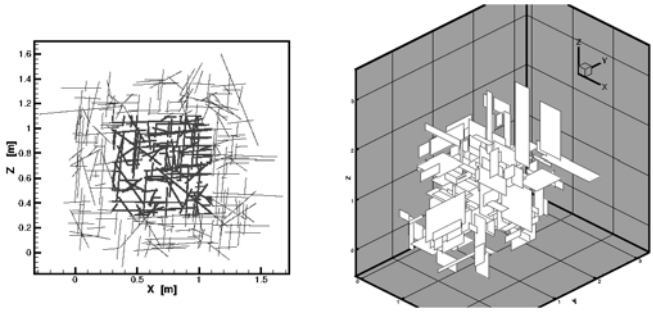

Fig. 2.13. Stochastically generated two- and three-dimensional fracture models.

The three-dimensional fracture generator FRAC3D was developed on the basis of the work of Long (1983), Long and Billaux (1987), and Wollrath (1990) A flow chart of the program algorithm can be seen in Fig. 2.14. Beside the fracture-generating routine itself, the program FRAC3D offers various methods for analyzing the quality of the generated fields, and for optimizing the generated fields. An interface for the mesh generation program ART and the flow and transport simulation program MUFTE-UG (see Sect. 2.4.4) is

included. A detailed description of the fracture generation program can be found in Silberhorn-Hemminger (2002).

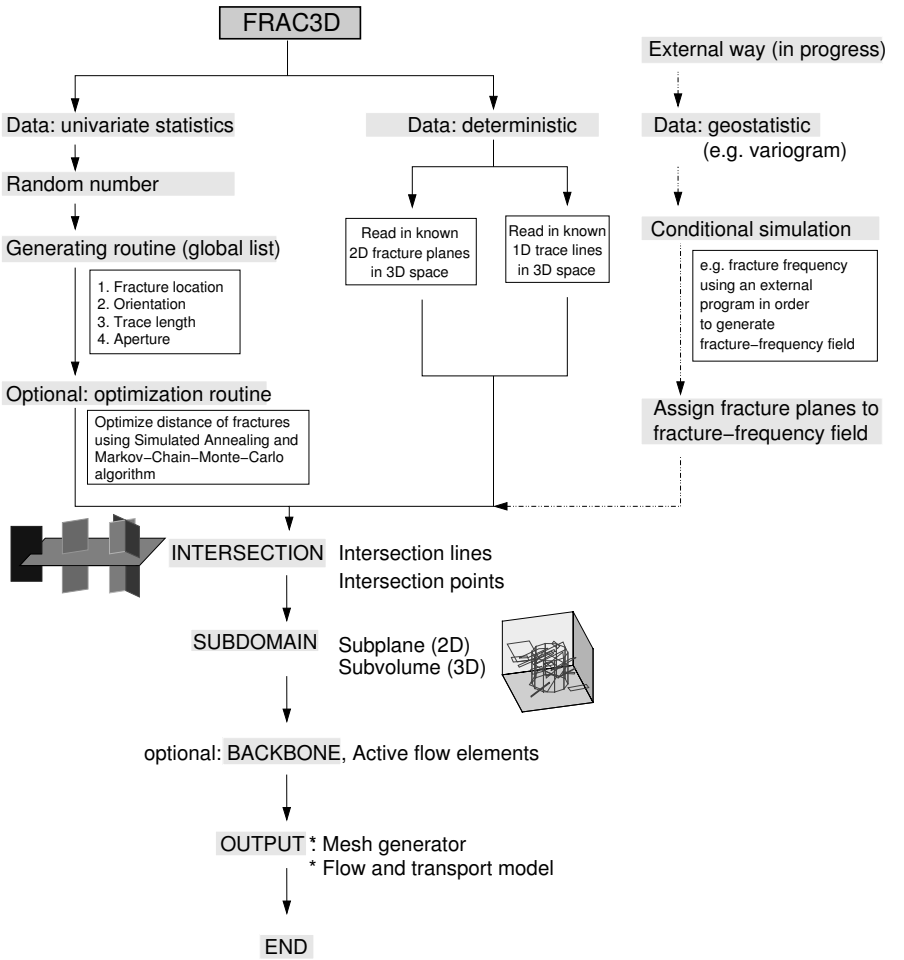

Fig. 2.14. Program algorithm of the fracture generator FRAC3D.

2.4.2.1 Generation Routine

As can be seen in Fig. 2.14, the algorithm for structure models for generating fractures is based on two different approaches: deterministic and stochastic. The choice of approach depends on the quantity and the quality of the input data available.

The deterministic approach requires exact information about a fracture network or a single fault zone. One of its main problems is that one has to

generate a three-dimensional system out of one- and two-dimensional information. Often, this approach is not feasible due to lack of information.

The second basic approach is the stochastic one. A large sample of fracture data (e.g. length, orientation) is required and a description of these field data by parameterized theoretical distributions, such as the FISHER distribution for the spherical orientation or the exponential distribution for the fracture lengths, must be available. It is important to be aware of the fact that these theoretical distributions are based on linear statistics. They do not include any information about the spatial variability of the data.

The generating routine includes the following steps:

```
while (simulated_fracture_density < target_fracture_density)
{
    step 1: Fracture location
            Generation of the mid point of fracture [i]
    step 2: Fracture orientation
            Generation of the normal vector of fracture [i]
    step 3: Fracture extension / length
            Generation of the spatial extension of
            fracture [i] and calculation of the four edge
            points of the fracture [i]
    step 4: Inclusion of the new generated fracture
            element [i] into the global list of all
            fracture elements
    step 5: Calculation of the simulated_fracture_density

    ++i
    total number of fractures: nfrac=i
}
```

An optional optimization routine for the parameter *fracture distance* completes the fracture generation.

The statistical characteristics of the newly generated fracture field are analyzed. For this purpose, the distribution functions of several fracture parameters are calculated. The difference between the input distribution functions and the distribution functions of the new field indicates the quality of the new field. If the differences are too large, the newly generated field is either rejected and the generation routine run again or the optimization routine starts.

2.4.2.2 Optimization

As the optimization routine, a *Simulated Annealing* algorithm followed by a *Markov-Chain-Monte-Carlo* algorithm is implemented in the fracture generator FRAC3D. The Simulated Annealing optimization step serves as a pre-

conditioning of the starting field for the subsequent Markov-Chain-Monte-Carlo optimization.

Because of the relatively smooth distributions of the fracture parameters *orientation* and *fracture length*, a good agreement between the input distributions and the distributions of the generated fields is generally achieved.

However, for the fracture parameter *fracture distance* an optimization is necessary since the information of the fracture distances cannot be taken into account in the generating routine described above. In order to include this important information in the generated fracture fields, a modified scanline technique is applied. The scanline technique allows the calculation of the fracture distance distribution and the optimization of the distribution.

2.4.2.3 Post-processing

In the next step, the intersection lines of the fracture planes and the intersection points of the intersection lines are determined (Fig. 2.15). Subsequently, the investigation domain is extracted from the generated domain (Fig. 2.16). Optionally, the inactive, disconnected fracture elements can be removed from the fracture network.

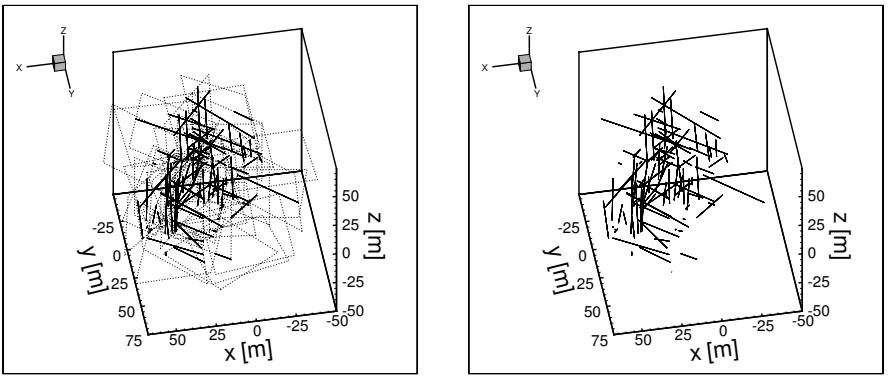

Fig. 2.15. Fracture network (left) and intersection lines (right).

Finally, the xyz-coordinates of the investigation domain, the fracture planes, the intersection lines, and the intersection points are converted into the data format required for the following mesh generation. Figure 2.17 shows a stochastically generated three-dimensional fracture network and two details of the finite element mesh of the fracture network. Fuchs (1999) gives detailed information about the mesh-generation program ART (Almost Regular Triangulation).

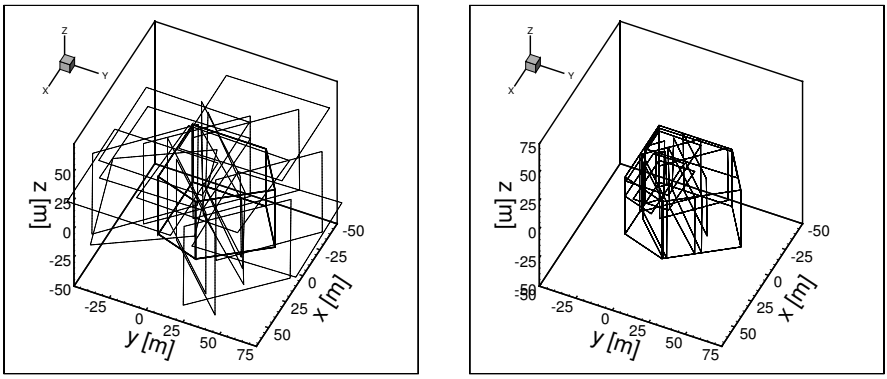

Fig. 2.16. Generated domain and extracted investigation domain.

2.4.2.4 Remarks

There is never a perfect match between a stochastic geometrical model and the real system on which it is based. It is possible to generate different realizations which are similar in their statistical description. However, one single realization can never exactly predict the behavior at a certain point of the real system. Therefore, one has to consider a large number of realizations. On the basis of these realizations, system properties such as the effective permeability and the effective dispersion of the system can be investigated and calculated (see e.g. Sect. 4.3.3). Additionally, one has to be aware of the fact that single fractures sometimes control the flow and transport processes in a fracture network completely by connecting different independent fracture clusters. If such dominating fractures are known and can be described by their orientation and extension, a combination of the deterministic and the stochastic approaches improves the reliability of the generated fracture network.

The generation approach discussed above incorporates deterministic and univariate stochastic information. A further improvement of the generation process is the implementation of routines for considering geostatistical information as well. Such algorithms are being developed as this book is being written. In Sect. 5.4, a geostatistical evaluation of the test site is discussed.

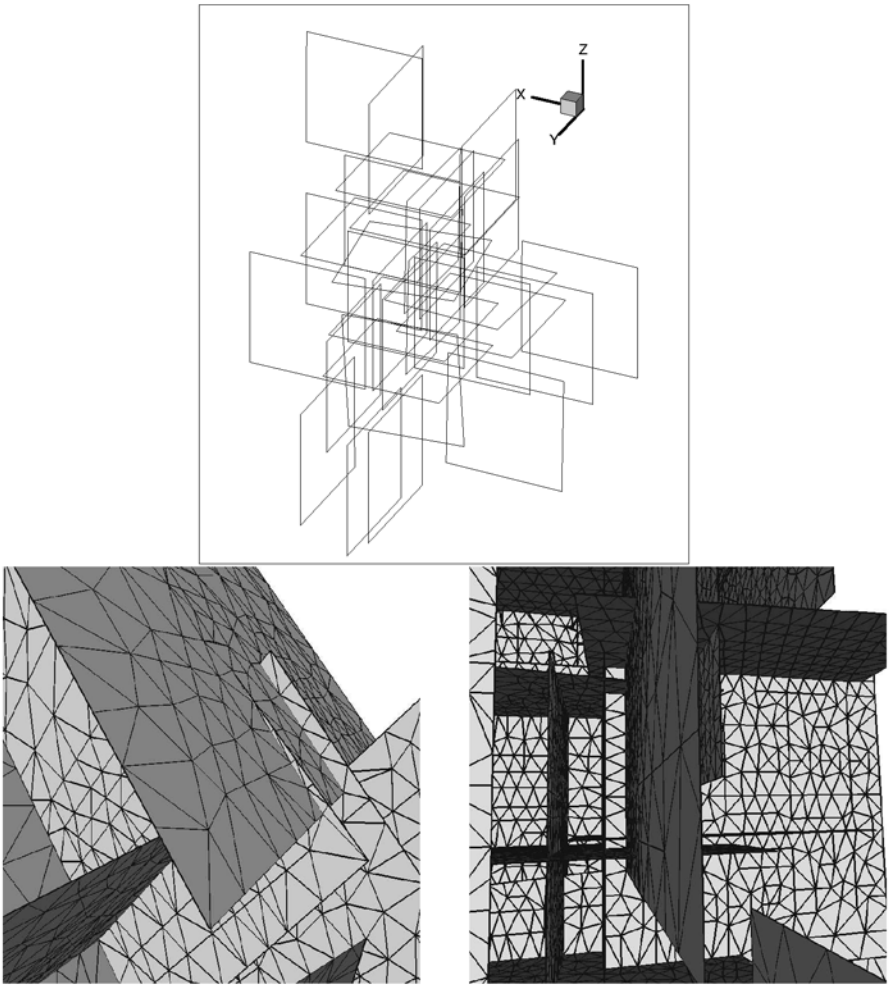

Fig. 2.17. Three-dimensional fracture network and details of the finite element mesh. Mesh generator ART (Almost Regular Triangulation) (Fuchs, 1999).

2.4.3 Spatial and Temporal Discretization

Due to the large discrepancy between the properties of the matrix and the fractures, large gradients occur in the vicinity of the fracture-matrix interface. To achieve an acceptable numerical accuracy, the mesh of the numerical model must have a high degree of refinement in these areas. Fractures may either be discretized with one dimension less than the matrix, i.e. as lines in a two-dimensional matrix or as a surface in a three-dimensional matrix, or with the same dimension as the surrounding matrix elements, i.e. equidimensionally (Fig. 2.18).

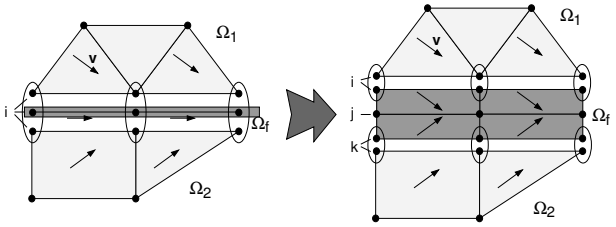

Fig. 2.18. Spatial discretization of a fracture embedded in a porous matrix in a two-dimensional domain. Left: Lower-dimensional discretization. Right: Equidimensional discretization. From Ochs *et al.* (2002).

For transport simulations, Neunhäuserer (2003) showed that the equidimensional approach yields a more accurate solution than the lower-dimensional one. However, the differences in the global solution are only significant if certain local effects accumulate in the system or if the processes are slow so that a relevant amount of tracer mass exchange occurs between the fracture and the matrix.

For time-dependent problems, sharp moving pressure and concentration fronts are obtained in the fractures, suggesting an adaptive refinement method in order to save computing time, especially for highly complex systems. The temporal discretization required is in general finer in the vicinity of the fractures, where very high flow velocities occur compared to the velocities in the surrounding matrix. An implicit temporal discretization is often chosen in order to achieve a stable solution, despite the wide range of velocities. The disadvantage of this approach is a significant influence of numerical dispersion.

Detailed discussions on spatial and temporal discretization methods can be found in, for example, Neunhäuserer (2003), Helmig (1997), Bastian *et al.* (1999), Kinzelbach (1992), and Hirsch (1984).

2.4.4 Applied Numerical Model – MUFTE-UG

The numerical model used for most discrete modeling investigation in this book is MUFTE-UG. It consists of the two parts: MUFTE (Multiphase Flow, Transport and Energy Model) and UG (Unstructured Grids). Figure 2.19 gives an overview of the features of the models. UG is a software toolbox providing techniques for the numerical solution of partial differential equations (PDEs) on unstructured grids (Bastian, 1997). For solving linear and nonlinear PDEs, several multi-grid solvers are available as well as adaptive and parallel techniques. MUFTE contains numerous discretization methods and applications for modeling non-isothermal multi-phase processes in porous and fractured media (Helmig (1997); Helmig *et al.* (1998)). Geometrically complex structures, such as fractures systems, can be simulated with MUFTE-UG due to the flexibility of the system and its compatibility with the powerful mesh generator ART (Fuchs, 1999).

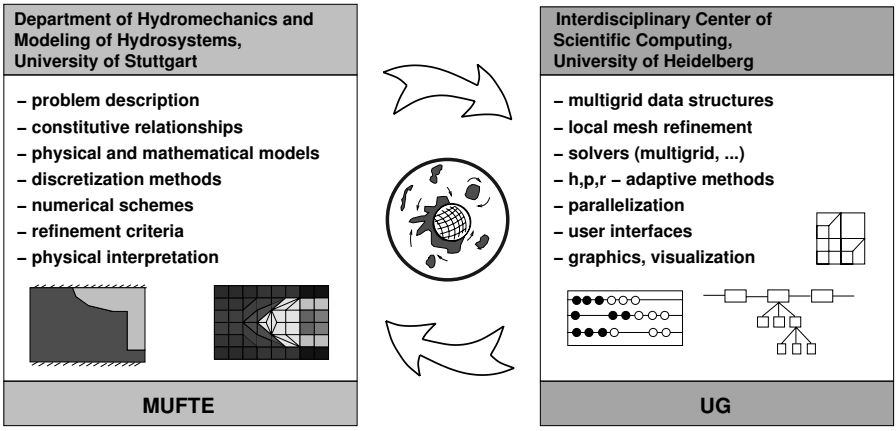

Fig. 2.19. Overview of the model system MUFTE-UG.

2.4.5 Summary

This section provides a rough overview of the discrete model concept as it is applied and implemented for the investigations within the framework of the research work presented in this book. It gives a basis for a better understanding of the simulation results presented and discussed later on.

Discrete modeling of fractured porous media requires not only an accurate approximation of the flow and transport processes in the matrix, within the fractures and at their interfaces but also the best possible description of the geometrical properties of the system.

The parallel-plate concept for the description of flow within the fractures is explained and the fracture generator FRAC3D presented. Possible spatial and temporal discretization methods are discussed briefly and the numerical model MUFTE-UG is introduced.

Typical numerical difficulties are not included here. Detailed discussions on this topic are given in, for example, Jakobs (2004), Reichenberger (2003), Neunhäuserer (2003) and Barlag (1997).

2.5 Implementation of the Multi-continuum Concept

T. Vogel, D. Jansen, J. Köngeter

The basic idea of multi-continuum modeling is to model separate, coupled hydraulic components of a heterogeneous aquifer. This principle of the multi-continuum model is illustrated in Fig. 2.20 for three identified continua. It is assumed that each component is distributed continuously in space and satisfies the conditions of a porous medium (Bear and Bachmat, 1990). For fracture matrix systems, this could be two fracture continua, such as a micro- and a macro-fracture system, and a matrix continuum with appropriate equivalent parameters (cf. Sect. 2.5.5).

A detailed modeling of such systems by a discrete model approach requires a high standard of modeling techniques and sufficient computer resources, as well as very detailed experimental investigations of the aquifer properties. Conversely, a representation of the aquifer by a single continuum model neglects the interactions between the components, which may be significant for the integral transport behavior of the aquifer. Multi-continuum models offer an efficient solution for this conflict.

The scale of interest (cf. Sect. 2.2) is the third zone (the far-field scale), where flow and transport may be considered to occur simultaneously, in overlapping continua. Single fractures are not observed to be dominant, as the mean length of the fractures is much smaller than the scale of interest.

It may seem that fewer input data are required for setting up a multi-continuum model than for the discrete approach (cf. Sect. 2.4). However, for high-quality multi-continuum modeling, a very good data basis is necessary. Data are needed so that hydraulically effective components and their interactions can be identified. An aquifer within fractured porous media with two components could be identified as double-porous and single-permeable (DPSP), double-porous and double-permeable (DPDP) or as single-porous and single-permeable (SPSP).

2.5.1 Governing Equations

The governing equations concerning flow and transport are formulated in the same way as for a porous medium (cf. Sect. 2.3) and are based on the

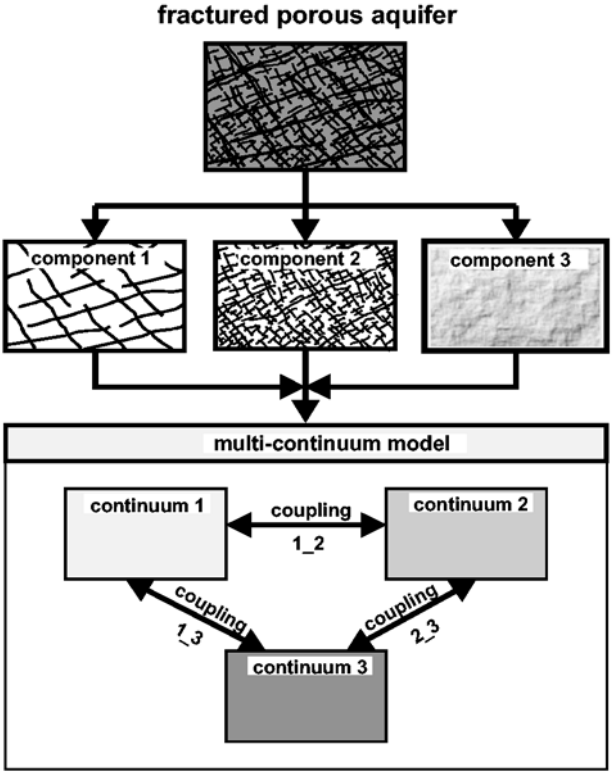

Fig. 2.20. Principle of the multi-continuum approach for fractured permeable formations (Jansen, 1999).

principle of conservation of mass. The multi-continuum approach requires a particular consideration of volume consistency and of exchange terms.

For the denomination of parameters and variables, the number of averaging processes is taken into account. Parameters with a single bar are equivalent continuum parameters and parameters with two bars are averaged over certain areas of the continuum. Equivalent parameters such as porosity are to be averaged once over the REV (cf. Sect. 2.3.1). An example of a second averaging is the averaging of the concentration distribution in a matrix block to obtain one equivalent mean value (cf. Fig. 2.21).

The equations for the continuum correspond to the equation for transient flow and the advection-dispersion equation for conservative tracers. In addition to the familiar terms (storage, flow, source and sink term, advection and dispersion terms), the exchange terms $W_{\alpha\beta}$ and the relative reference volumes Φ_α have to be considered. The latter transform the governing equations for the continuum based on the natural volume of this component. The

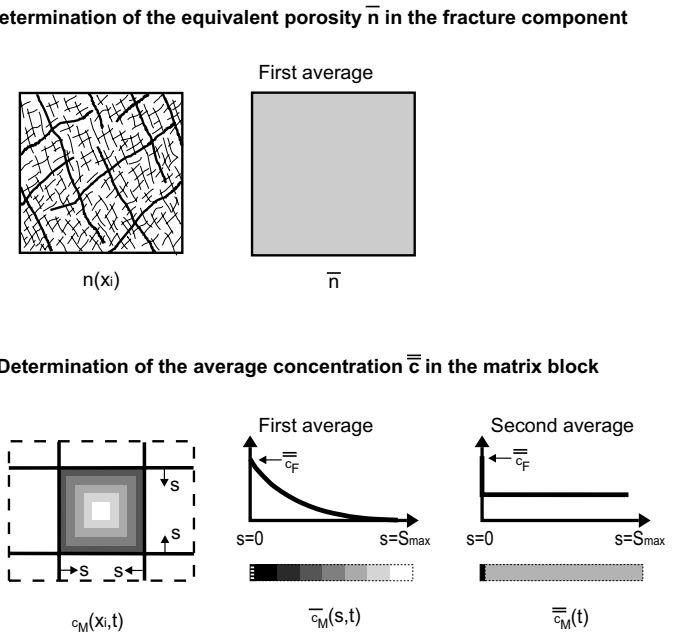

Fig. 2.21. Determination of the first and second average of parameters over certain areas of the continuum (Jansen, 1999).

following equations apply to the continuum α. The index β denotes the continuum coupled with α.

The equation for the flow field, formulated for the hydraulic head as variable, is thus expressed for the permeable component as follows:

$$\Phi_\alpha \left(\bar{S}_{\mathrm{S},\alpha} \frac{\partial \bar{\bar{h}}_\alpha}{\partial t} - \frac{\partial}{\partial x_i} \bar{K}_{ij,\alpha} \frac{\partial \bar{\bar{h}}_\alpha}{\partial x_j} + \bar{Q}_{\mathrm{Q,S},\alpha} \right) + \Phi_\alpha \Phi_\beta W_{\mathrm{Ql},\alpha\beta} = 0 \,. \tag{2.39}$$

Transport processes within a permeable component are modeled by solving the advection-dispersion equation (2.40):

$$\begin{aligned} &\Phi_\alpha \left(\bar{n}_{e,\alpha} \frac{\partial \bar{\bar{c}}_\alpha}{\partial t} + \bar{\bar{q}}_{i,\alpha} \frac{\partial \bar{\bar{c}}_\alpha}{\partial x_i} - \frac{\partial}{\partial x_i} \bar{\bar{D}}_{ij,\alpha} \frac{\partial \bar{\bar{c}}_\alpha}{\partial x_j} + \bar{Q}_{Q,S,\alpha} (c_R - \bar{\bar{c}}_\alpha) \right) \\ &+ \Phi_\alpha \Phi_\beta W_{c,\alpha\beta} = 0 \,. \end{aligned} \tag{2.40}$$

Within this formulation, $\bar{n}_{e,\alpha}$ is the equivalent porosity and $\bar{\bar{q}}_{i,\alpha}$ is the DARCY velocity. $\bar{\bar{D}}_{ij}$ is the tensor of hydrodynamic dispersion (cf. Sect. 2.3.3.2) in this context, written as

$$\bar{\bar{D}}_{ij} = \bar{\alpha}_t \delta_{ij} |q_{ij}| + (\bar{\alpha}_l - \bar{\alpha}_t) \frac{\bar{\bar{q}}_i \bar{\bar{q}}_j}{|\bar{\bar{q}}|} + \bar{n} \bar{D}_{\mathrm{m},ij} \,. \tag{2.41}$$

$\bar{Q}_{Q,S,\alpha}(c_R - \bar{\bar{c}}_\alpha)$ is a source or sink term and W_c is the exchange of mass between the coupled continua α and β. If all exchange processes are taken into account, W_c is given by equation (2.42):

$$W_{c,\alpha\beta} = W_{Dl,\alpha\beta} + W_{Al,\alpha\beta} + W_{Ar,\alpha\beta} \; . \tag{2.42}$$

W_{Dl} is the diffusive solute exchange due to a concentration gradient between the two components. W_{Al} and W_{Ar} are exchange masses due to local and regional advection respectively. The local advection is caused by a fluid exchange resulting from a transient flow, where the tracer is transported advectivly between the coupled continua. If the flow within the subordinate component (e.g. matrix component) is not negligible, a mixing of the flows may occur at the fracture-matrix interface, leading to an exchange of tracer mass. This mixing is represented by the regional advection term (cf. Fig. 2.22).

2.5.2 Types of Coupling

The characteristics of a multi-continuum model are described by the number of identified hydraulic components and the type of coupling and exchange formulation between the continua (cf. Fig. 2.25). The different coupling methods are either parallel, serial or selective (cf. Fig. 2.23). A parallel coupling means that all identified continua are coupled with each other directly, as shown by Gwo *et al.* (1995). A serial coupling (e.g. Lee and Tan, 1987) implies a coupling in the order of hydraulic conductivity (i.e. macro-fracture system, micro-fracture system and matrix). The selective coupling (e.g. Closmann, 1975) would, for example, couple the macro-fracture system to the micro-fracture system and to the matrix, but would not couple the micro-fracture system and the matrix.

2.5.3 Exchange Formulation

Besides the coupling method of the total system, the exchange formulation chosen for the single couplings is important (cf. Fig. 2.25). In the following, double-continuum models are considered, representing two coupled components of a multi-continuum model. The type of continuum model (DPSP or DPDP) defines the appropriate exchange model. Transient approaches (Bertin and Panfiloy (2000), Moyne (1997), Zimmermann *et al.* (1993), Pruess and Narasimhan (1985), among others) and quasi-steady formulations (Quintard and Whitaker (1996), Kazemi (1969),Warren and Root (1963), Barenblatt *et al.* (1960), among others) can be distinguished.

2.5.3.1 DPSP Models with Transient Exchange Formulation

If DPSP models are considered, only molecular diffusion (matrix diffusion), which is of a local nature and does not depend on regional processes, is mod-

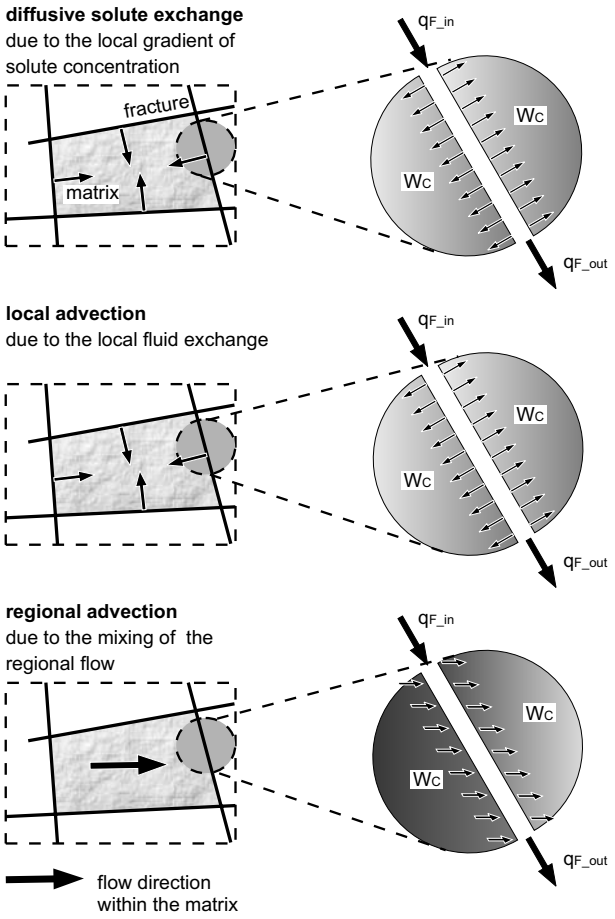

Fig. 2.22. Possible exchange processes for the components (Jansen, 1999).

eled for the matrix. Making use of the local nature of matrix diffusion, transport in the matrix is described by the local one-dimensional diffusion equation (2.43)

$$n_{\mathrm{e},\beta}\frac{\partial c_\beta}{\partial t} - \frac{1}{A_\beta(s)} n_{\mathrm{e},\beta} D_{\mathrm{m},\beta}\frac{\partial}{\partial s}\left(A_\beta(s)\frac{\partial c_\beta}{\partial s}\right) + Q_\beta(c_R - c_\beta) = 0\,, \qquad (2.43)$$

where s is the distance from the exchange interface (the matrix block surface), $A(s)$ is the interface area for diffusive flux at this distance and D_{m} is the molecular diffusion coefficient. Formulations for $A(s)$ are given by Pruess and Karasaki (1982) and Jansen *et al.* (1996). Within the specific surface to volume ratio of the porous blocks Ω_0, W_{D} is given by FICK's law:

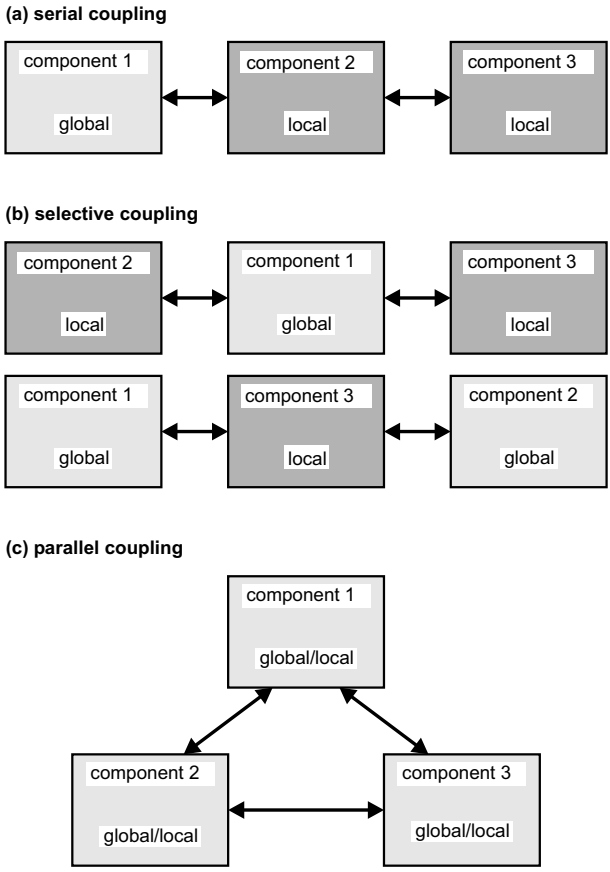

Fig. 2.23. Serial (a), selective (b) and parallel (c) coupling of hydraulic components.

$$W_{\mathrm{D},\alpha\beta} = -\bar{\Omega}_{0,\beta}\bar{n}_{\mathrm{e},\beta}\bar{D}_{\mathrm{m},\beta}\left.\frac{\partial \bar{c}_\beta}{\partial s}\right|_{s=0.0}. \tag{2.44}$$

2.5.3.2 DPDP Models with Quasi-Steady Exchange Formulation

If regional transport is considered in both coupled continua, exchange processes are no longer only of a local nature. Therefore, equation (2.40) must be solved for both continua.

The quasi-steady formulation describing the solute exchange W_c can be written for the fluid exchange as follows:

$$W_{\mathrm{Qr},\alpha\beta} = |\bar{\Omega}_{W,ij,\alpha\beta}\,\bar{\bar{q}}_{i,\beta}| \tag{2.45}$$

$$W_{\mathrm{Ql},\alpha\beta} = \bar{\Omega}^2_{0,\beta}\bar{\alpha}_{\mathrm{Q},\beta}(\bar{\bar{h}}_\alpha - \bar{\bar{h}}_\beta) \tag{2.46}$$

and for the solute exchange as

$$W_{\mathrm{Dl},\alpha\beta} = \bar{\Omega}^2_{0,\beta}\bar{\alpha}_{\mathrm{c},\beta}(\bar{\bar{c}}_\alpha - \bar{\bar{c}}_\beta) \tag{2.47}$$

$$W_{\mathrm{Al},\alpha\beta} = |W_{\mathrm{Ql},\alpha\beta}|(\bar{\bar{c}}_\alpha - \bar{\bar{c}}_\beta) \tag{2.48}$$

$$W_{\mathrm{Ar},\alpha\beta} = |W_{\mathrm{Qr},\alpha\beta}|(\bar{\bar{c}}_\alpha - \bar{\bar{c}}_\beta)\ . \tag{2.49}$$

In equation (2.48), W_{Ql} is the fluid exchange due to the local pressure gradient between continuum α and β. In equation (2.49), W_{Qr} is the fluid exchange due to the mixing of fluxes. Procedures for determining W_{Qr} are presented in Jansen (1999). Ω_{W} is the surface function that describes the relevant part of the fracture for mixing. Figure 2.24 illustrates how exchange processes between two components depend on direction. The regional hydraulic gradient induces a fluid flow in the fracture and the matrix system. The direction of flow, e_{qM}, in the matrix system is in accordance with the conductivity characteristics. Inside the fracture, flow is possible only in the direction of the fracture axis. If the flow in the matrix system is perpendicular to a fracture, the regional mass exchange is maximal. If the flow in the matrix system is parallel to the direction of flow in the fracture, the two flows do not mix. Thus, the intensity of mixing of the two flows depends on their relative orientation and magnitude.

The specific fracture surface $\Omega_W(e_{qM})$ is the measure for the surface of interaction participating in the regional fluid exchange. It is defined as the

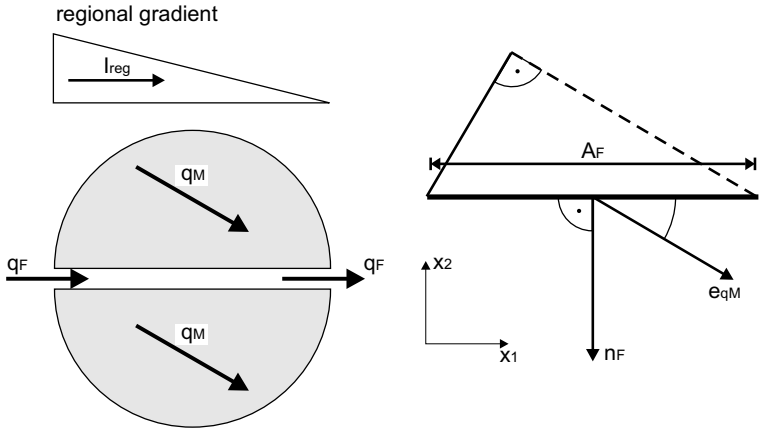

Fig. 2.24. Dependence of regional exchange processes on flow direction (Jansen, 1999).

ratio of the sum of the perpendicular projections of all N fracture surfaces A_F to the direction of flow e_{qM} in the matrix and the volume V_M of the total system under consideration:

$$\Omega_W(e_{qM}) = \frac{1}{V_M} \sum_{k=1}^{N} A_F(k) e_{qM} n_F(k) \ . \tag{2.50}$$

Ω_W can be obtained by a best-fit analysis. The exchange parameters $\bar{\alpha}_c$ and $\bar{\alpha}_Q$ have to be calibrated.

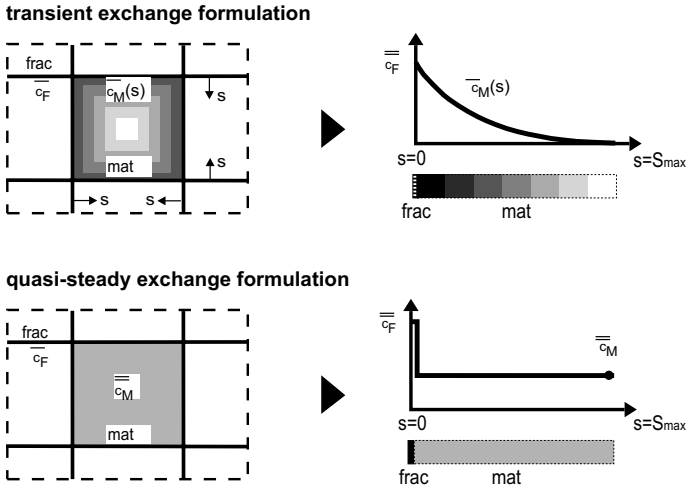

Fig. 2.25. Transient and quasi-steady exchange formulations (Jansen *et al.*, 1998).

2.5.4 Numerical Model

The numerical model STRAFE was developed by the Institute of Hydraulic Engineering and Water Resources Management, Aachen University. The following list provides an overview of the characteristics of the STRAFE multi-continuum model used for the investigations in this book:

- the number of components is theoretically infinite;
- permeable components can only be modeled globally;
- porous components can be modeled locally or globally;
- two permeable components are coupled with the quasi-steady exchange formulation;
- the coupling of a permeable and a porous component can be performed with the quasi-steady exchange formulation or the transient formulation;

- simultaneous coupling of several components can be done in a parallel, serial or selective way;
- the numerical solution is achieved by the standard Galerkin Finite Element method;
- a combination of one-, two- or three-dimensional finite elements is possible.

Birkhölzer (1994b) and Jansen (1999) have presented very detailed descriptions of the numerical model. For the evaluation of flow and transport processes in the unsaturated zone, STRAFE has been further developed to handle these processes in multi-continuum systems by taking the RICHARDS equation into account (Lagendijk (1997) and Thielen (2002)).

2.5.5 Determination of Equivalent Parameters

In the following sections, methods for determining equivalent parameters are presented. These methods are used to obtain parameter sets that are necessary to set up a multi-continuum model as described in the previous section. Applications of these methods are described later in this book (e.g. Chapter 4).

2.5.5.1 Tensor of Equivalent Hydraulic Conductivity

The equivalent hydraulic conductivity tensor describes the flow properties of a fractured and/or porous medium, determined by an averaging process over the corresponding REV. The determination of the hydraulic conductivity tensor is performed according to Long (1983) and Wollrath (1990): a hydraulic gradient is imposed on the system under investigation with varying angles and the corresponding discharge is established (Fig. 2.26, left). The equivalent hydraulic conductivity for each direction is calculated as

$$K_\gamma \;=\; \frac{Q_\gamma}{A \;\cdot\; \mathrm{grad}(h_\gamma)}, \tag{2.51}$$

where γ is the direction, K is the equivalent hydraulic conductivity, Q is the discharge, A is the area of the outflow boundary and $\mathrm{grad}(h_\gamma)$ is the imposed hydraulic gradient. With the least-square method, an ellipse is fitted to the collection of directional values, representing the equivalent hydraulic conductivity tensor of the system (Fig. 2.26, right).

$$K_\gamma \;=\; \underline{e}^T \,\underline{\underline{K}}\, \underline{e} \qquad \text{with} \quad \underline{e} \;=\; \begin{bmatrix} cos\ \gamma \\ sin\ \gamma \end{bmatrix} \tag{2.52}$$

The better the directional hydraulic conductivities fit the ellipse, the closer the system is to an REV and the better its flow processes can be described by a continuum with the properties of the determined equivalent tensor.

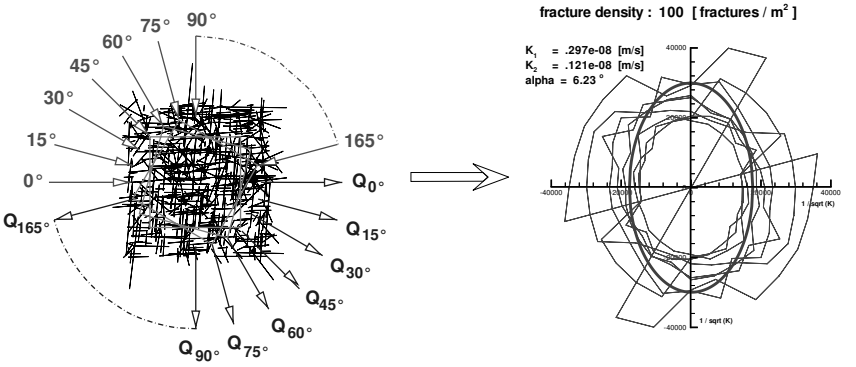

Fig. 2.26. Fracture system and directional discharges (left). Calculated hydraulic conductivities (right) for different fracture system realizations and fitted ellipse (Hemminger *et al.*, 1998).

2.5.5.2 Equivalent Porosity

To describe the mean transport characteristics of a medium, the equivalent porosity $\overline{n}$ is ascertained. The procedure is based on the same principle as for the determination of the tensor of equivalent hydraulic conductivity (cf. Sect. 2.5.5.1).

For each angle γ in which a hydraulic gradient is applied to the system, a transport calculation is performed (Fig. 2.26, left). At the input boundary, a known quantity of an ideal tracer is introduced into the system. At the output boundary, the breakthrough curve is determined and the corresponding cumulative curve is calculated. The equivalent porosity $\overline{n}$ of the system is obtained by:

$$\bar{n}_\gamma = \frac{Q_\gamma t_{\text{median}}}{V} \,. \tag{2.53}$$

The parameter $\bar{n}_\gamma$ is the directional equivalent porosity, Q_γ is the directional discharge, and V is the volume of the total system. t_{median} is the point in time at which 50 % of the tracer mass are detected at the outflow boundary.

Here, only volumes are considered, since the ratio of the volume occupied by flow processes to the total volume is calculated. Initially, the porosity is regarded as being directional, as it is determined on the basis of a breakthrough curve corresponding to a certain direction. It goes without saying that for the calculations, the porosity is considered to be independent of direction and is thus a scalar quantity.

2.5.5.3 Tensor of Equivalent Dispersivity

In order to derive the equivalent dispersion tensor $D_{\text{d},ij}$, first the directional dispersivity $\alpha_{\text{l},\gamma}$ is determined for each of the tracer breakthrough curves.

The determination is based on the one-dimensional transport equation for a DIRAC impulse:

$$c\left(x,t,\alpha_{l,\gamma}\right) = \frac{\Delta M}{2\, n_{e,\gamma}\, b\, m\, \sqrt{\pi\, \underline{v}\, t\, \alpha_{l,\gamma}}} \cdot exp\left[-\frac{(x - \underline{v}\, t)^2}{4\, \underline{v}\, t\, \alpha_{l,\gamma}}\right]. \qquad (2.54)$$

Here, c is the concentration, x is (in this case) the distance between the in- and the outflow boundary, t is the time, ΔM is the injected tracer mass, $n_{e,\gamma}$ is the directional porosity, b the width of the area, m the thickness of the domain, $\underline{v}$ is the mean seepage velocity and $\alpha_{l,\gamma}$ is the directional dispersivity to be determined. With equation (2.54), the $\alpha_{l,\gamma}$ yielding the best reproduction of each of the tracer breakthrough curves is iteratively obtained. For this purpose, the equation is solved with gradually varying $\alpha_{l,\gamma}$ and the deviation from the simulated curve is derived using the least-square method, where N is the number of time sampling points of the tracer breakthrough curve:

$$E = \sum_{i=1}^{N} \left(c_{sim,i} - c\left(x,t_i,\alpha_{l,\gamma}\right)\right)^2. \qquad (2.55)$$

The error is plotted over $\alpha_{l,\gamma}$ and the minimum is established.

From the determined directional dispersion lengths, the directional dispersion coefficient D_γ can be ascertained using the corresponding seepage velocity. The dispersion tensor is established according to the same procedure as for the determination of the hydraulic conductivity (cf. Fig. 2.26). From the principal axes of the tensor, the equivalent longitudinal and transversal dispersion for the angle between the first principal axis and the polar axis can be determined. This concept yields an approximated reference value for the directional dispersivity. The disadvantage of this rather simple approach is that early concentration peaks and strong tailing, both very typical characteristics of the tracer breakthrough curves of fractured porous systems, are not satisfactorily reproduced.

2.5.6 Characteristic Values

Birkhölzer (1994a) and Jansen (1999) develop characteristic values in order to evaluate the importance of exchange processes and to assess the integral transport behavior of the model. A good approximation of characteristic values is necessary to choose an appropriate type of exchange model and to identify the relevant parameters of the aquifer.

As the multi-continuum model presented here allows for both a coupling of fracture-matrix systems and fracture-fracture systems, two conceptual systems are investigated to identify the characteristic values.

Berkowitz *et al.* (1988) present an idealized model area that consists of a regularly fractured fracture network and uniform matrix blocks. The model area and boundary conditions are illustrated in Figure 2.27.

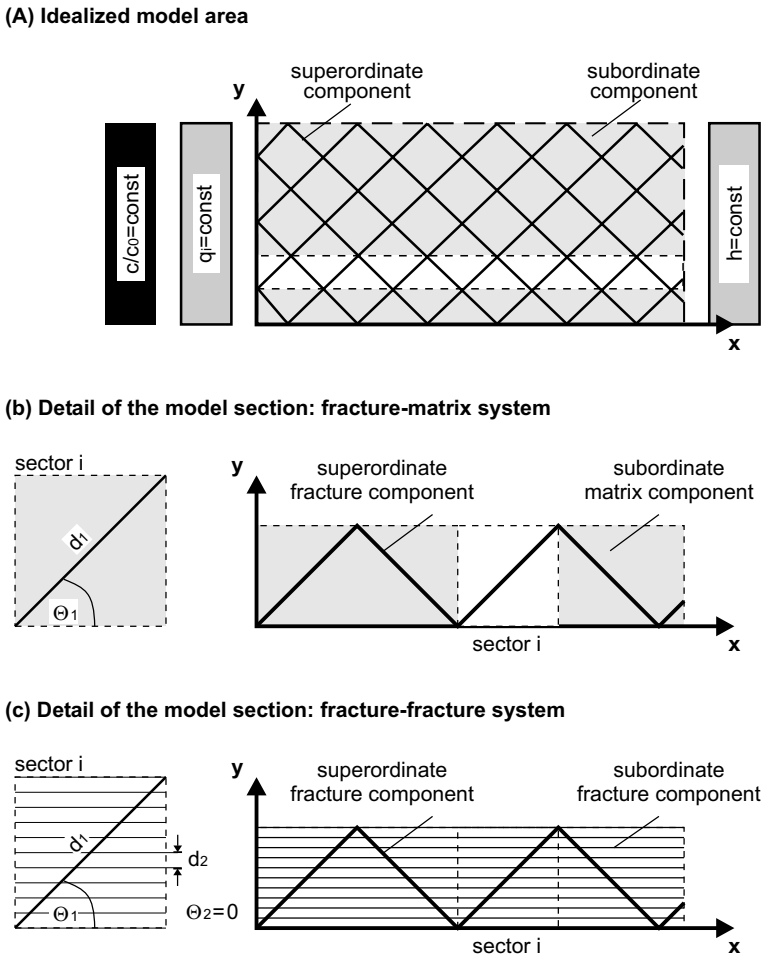

Fig. 2.27. Idealized model area to identify the characteristic values (Jansen, 1999).

The superordinate component consists of two fracture sets that are inclined by θ_1 and $-\theta_1$ respectively. These matrix blocks are quadratic with a side length of d_1 that are supposed to be isotropic and homogeneous. The fracture spacing d_1 and the fracture aperture of $\bar{b}_1$ are assumed to be constant. The subordinate fracture set of the fracture-fracture system consists of horizontal fractures with a spacing of d_2 and an aperture of $\bar{b}_2$.

For the confined model area, steady-state flow conditions are assumed. Continuous tracer injection is performed on the left model boundary.

A regional flow in the direction of the x-axis occurs due to the model area and boundary conditions. This flow field does not cause a dispersive tracer

flow at the fracture intersections. Thus, the model area may be reduced to a strip of $d_1 cos\,\theta_1$ in height and a length x.

2.5.6.1 Mobility Number

The mobility number N_{M} is defined as the ratio of the equivalent DARCY velocity of the subordinate component β and the superordinate component α:

$$N_{\mathrm{M}} = \frac{q_\beta}{q_\alpha} \,. \tag{2.56}$$

It allows for a characterization of the coupled components with regard to the mobility of the fluid in the subordinate component and is therefore a significant criterion on for choosing between a storage or mobility approach.

In the case of isotropic flow conditions and a hydraulic gradient in the x-direction considered here, the mobility number of the fracture-matrix system is defined as

$$N_{\mathrm{M}} = \frac{q_{x,2}}{q_{x,1}} = \frac{K_f}{\frac{g}{6\nu}\frac{(\bar{b}_1)^3}{d_1} cos^2\theta_1} \,, \tag{2.57}$$

whereas, for the fracture-fracture system it is defined as:

$$N_{\mathrm{M}} = \frac{q_{x,2}}{q_{x,1}} = \frac{1}{2}\left(\frac{\bar{b}_2}{\bar{b}_1}\right)^3 \frac{d_1 cos^2\theta_2}{d_2 cos^2\theta_1} \,. \tag{2.58}$$

In order to evaluate the mobility of the fluid in the subordinate component, the relevant parameters for a fracture-matrix system are, according to equation (2.57), the equivalent hydraulic conductivity of the matrix, the fracture width and fracture density of the superordinate component, as well as the orientation of the fractures to the hydraulic gradient.

The flow regime in fracture-fracture systems is determined according to equation (2.58) by the ratio of the fracture width, the ratio of the fracture densities and the ratio of the orientation to the hydraulic gradient.

The reciprocal value of the fracture distances is equal to the fracture density of parallel fractures which is defined as the number of fractures per unit area (Long *et al.*, 1982). Fracture densities are used here because they may also be applied to irregular fracture networks.

2.5.6.2 Diffusion-Advection Number

The diffusion-advection number N_{DA} is defined as the ratio of mass transferred in a diffusive and regional-advective way:

$$N_{\mathrm{DA}} = \frac{M_D}{M_{Ar}} \,. \tag{2.59}$$

This parameter allows for the characterization of the importance of exchange processes. It is defined for steady-state flow conditions, where mass transfer due to local advection does not occur.

The diffusive mass transport in the subordinate component results from the spatial and temporal integration of the FICK's second law:

$$\frac{\partial C}{\partial t} = D_{\mathrm{m},2} \frac{\partial^2 C}{\partial s^2} \,, \tag{2.60}$$

leading to

$$M_D = C_0 n_2 \sqrt{8 D_{\mathrm{m},2} T} dA \,, \tag{2.61}$$

where the equivalent porosity of the subordinate fracture component is defined as:

$$n_2 = \frac{\bar{b}_2}{d_2} \,. \tag{2.62}$$

Concerning the advective mass transport, only the perpendicular projection $sin\,\theta_1 dA$ in the direction of the flow q_2 is relevant. The mass transferred advectively in the subordinate component during the time T thus results in:

$$M_{Ar} = C_0 q_2 T sin\,\theta_1 dA \,. \tag{2.63}$$

Taking the flow velocities into account, the diffusion-advection number of the fracture-matrix system is defined as

$$N_{\mathrm{DA}}(T) = \frac{M_D}{M_{Ar}} = \frac{n_2}{K_f I_x sin\,\theta_1} \sqrt{\frac{8 D_{\mathrm{m},2}}{T}} \tag{2.64}$$

and, for the fracture-fracture system, one obtains:

$$N_{\mathrm{DA}}(T) = \frac{M_D}{M_{Ar}} = \frac{12\nu}{g \bar{b}_2^2 cos^2\theta_2 I_x sin\,\theta_1} \sqrt{\frac{8 D_{\mathrm{m},2}}{T}} \,. \tag{2.65}$$

Interpreting the importance of mass-exchange processes by the diffusion-advection number leads to the same parameters of the discrete system as for the mobility number (cf. Sect. 2.5.6.1). Additionally, the time scale is taken into account. At early points in time, the gradient of concentration at the block surface is very steep, resulting in a high diffusive mass exchange and a maximum value for N_{DA}. Later, the concentration gradient decreases and the diffusion-advection number exhibits a smaller value. As a characteristic point in time, the loading time T^* is suggested.

2.5.6.3 Loading Time

The loading time T^* is a characteristic time scale describing the period of interaction between the components. In order to determine T^*, both advective and diffusive processes are considered. T^* is defined to account for the time a tracer particle takes to move the distance s_{max} (penetration depth) from the block surface to the middle of the block advectively during the time T_A^* and diffusively during the time T_D^* respectively:

$$T^* = \left(\frac{1}{T_A^*} + \frac{1}{T_D^*} \right)^{-1} . \tag{2.66}$$

The maximum advective transport distance from the block surface to the center of the block is expressed by

$$s_{\max,A} = d1 cos\, \theta_1 . \tag{2.67}$$

The pore velocity within the matrix component is defined as

$$v_{x,2} = \frac{K_f I_x}{n_2} , \tag{2.68}$$

and, for the subordinate fracture component,

$$v_{x,2} = \frac{1}{n_T} \frac{g}{12\nu} \bar{b}_2^2 cos^2\theta_2 I_x , \tag{2.69}$$

where n_T is the porosity of the fracture filling. The advective loading time T_A^* is therefore defined for the matrix component as

$$T_A^* = \frac{n_2 d_1 cos\, \theta_1}{K_f I_x} \tag{2.70}$$

and as

$$T_A^* = \frac{n_t 12\nu d_1 cos\, \theta_1}{g \bar{b}_2^2 cos^2\theta_2 I_x} \tag{2.71}$$

for the fracture component. The diffusive transport distance perpendicular to the block surface is defined for a matrix component as

$$s_{\max,D} = d_1 sin\, \theta_1 . \tag{2.72}$$

Within the subordinate fracture component, diffusive solute transport may only occur in the direction of the fractures. The diffusive transport distance to the center of the block may thus be determined as

$$s_{\max,D} = d_1 cos\, \theta_1 . \tag{2.73}$$

Therefore, the diffusive loading time of a matrix component is

$$T_D^* = \left(\frac{1}{2} d_1 sin\, 2\theta_1\right)^2 \frac{1}{2D_{\mathrm{m},2}} \tag{2.74}$$

and

$$T_D^* = \left(d_1 cos\, \theta_1\right)^2 \frac{1}{2D_{\mathrm{mol},2}} \tag{2.75}$$

for a subordinate fracture component.

Comparing the loading times for a fracture-matrix system and a fracture-fracture system, special attention has to be given to the equivalent porosity of a matrix and a fracture component because of their different orders of magnitude. The equivalent porosity of a matrix component is, in general, much higher than for a fracture component. Therefore, the relevant time scales for the exchange processes of fracture-matrix and fracture-fracture systems differ.

2.5.6.4 Loss of Identity Length

The loss of identity length L^* is a characterisitic length scale. It is used to estimate the transport distance within which a distinction between the two components is necessary. It is defined by an empirical approach and specifies the transport distance within which the concentration in the superordinate component, introduced at the input boundary, is dissipated to 0.1 % of the initial value, due to exchange processes with the subordinate component. There is a distinction between the advective loss of identity length L_A^* and the diffusive loss of identity length L_D^*, which are calculated as the loss of identity length exclusively for regional advection and diffusive mass exchange respectively. The loss of identity length is defined as:

$$L^* = \left(\frac{1}{L_A^*} + \frac{1}{L_D^*}\right)^{-1} . \tag{2.76}$$

Birkhölzer (1994a) expresses the term for the advective loss of identity length by:

$$L_A^* = -\frac{\ln 0.001}{N_{\mathrm{M}}} . \tag{2.77}$$

According to Tang *et al.* (1981) the diffusive loss of identity length L_D^* is estimated by means of the analytical solution of the diffusion of a tracer from a single fracture into an infinite half space. Making use of the simplification that adsorption and degradation processes can be neglected, the following equation is established:

$$\frac{c}{c_0} = 2\frac{exp(vz)}{\sqrt{\pi}} \int_l^\infty exp(-\xi^2 - \frac{v^2 z^2}{4\xi^2}) erfc\left(\frac{Y}{2T}\right) d\xi \tag{2.78}$$

with:

$$v = \frac{v_1}{2D_1} \tag{2.79}$$

$$Y = \frac{v^2\beta^2 z^2}{4A}\xi^{-2} \quad \text{with} \quad \beta^2 = \frac{4D_1}{v^2} \quad \text{and} \quad A = \frac{b}{n_2\sqrt{D_2}} \tag{2.80}$$

$$T = \sqrt{t - \frac{z^2}{4D_1}\xi^{-2}} \tag{2.81}$$

$$l = \frac{z}{2}\frac{1}{\sqrt{D_1 t}} \tag{2.82}$$

$$D_1 = v_1\alpha_l + D_\mathrm{m} \tag{2.83}$$

$$D_2 = \tau D_\mathrm{m} \; . \tag{2.84}$$

z characterizes the transport distance, v_1 is the pore velocity and D_1 the coefficient of dispersion in the fracture. The effective coefficient of molecular diffusion in the matrix is described by D_2 and the tortuosity in the matrix is defined as τ. The period of the observation is t.

By means of equation (2.78), the concentration profiles along the fracture axis are determined for specific points in time (Fig. 2.28). The transport length for which the concentration is equal to 0.1 % of the concentration at the input boundary can be deduced from these profiles. Birkhölzer (1994a) proposes a value of $0.2T_D^*$ as the period of observation. T_D^* is the diffusive loading time of a component. A detailed derivation of this parameter can be found in Birkhölzer (1994a).

2.5.7 Summary

Whereas Sect. 2.4 presents the discrete model concept, this section gives an overview of the alternative multi-continuum model concept. Additionally, necessary equivalent parameters are defined and the determination of these parameters is explained. Characteristic values quantifying the exchange processes in hydraulic systems with more than one component are introduced and their derivation is shown based on a idealized model area. This allows for a better understanding of the numerical investigations presented and discussed within this book.

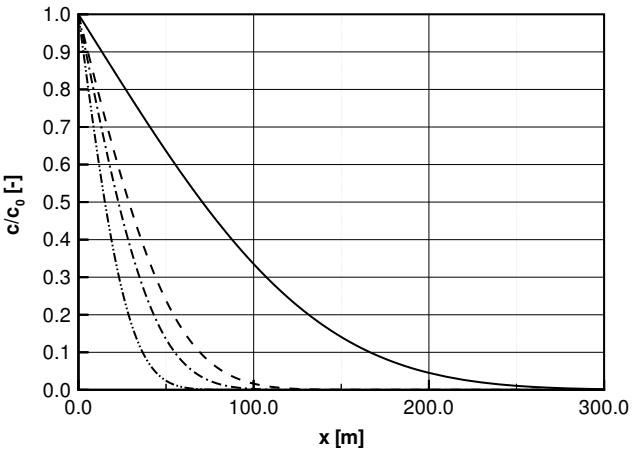

Fig. 2.28. Typical concentration profiles along the fracture for different points in time (Tang *et al.*, 1981).

Multi-continuum models, as a compromise between a detailed discrete approach and a simplified single-continuum approach, substitute the heterogeneous structure of an aquifer by overlaying, coupled homogeneous components that are continuously distributed in the model domain. Special attention has to be paid to the exchange processes and the related coupling terms.

Even though a multi-continuum approach is more general than a discrete model, a basis of solid and reliable experimental data is critical for the success of the model.

2.6 Summary

Following the steps of the transformation from a complex natural system to a simplified numerical model, general characteristics of fractured porous systems, the basic theory and concepts of flow and transport processes in such systems, and two different model approaches are presented.

The discussion has the objective of founding a basis for a better understanding of the research results presented in this book in later chapters.

The general properties of the components of fractured porous systems and in particular the geometrical characterization, often based on statistical approaches, are described.

A basic physical-mathematical description of single-phase flow and transport processes in porous media is given, relevant to the issues discussed in this book.

Depending on the problem scale, the types of heterogeneities (e.g. faults, fractures, fissures) and their frequencies, two different model approaches for the consideration of fractures in porous domains are proposed.

In a discrete model, the matrix and the fractures are locally idealized as continua and the fractures are implemented discretely at their actual location within the domain. Due to the extensive property and geometrical data requirements, as well as the high spatial and temporal resolution necessary to obtain accurate results, discrete models are best suited for principal investigations on a limited scale.

The second approach introduced is the multi-continuum model approach. By transforming, for example, the matrix and the fractures on different scales into separate equivalent continua, the domain is partly homogenized. The exchange between the defined continua is realized by introducing exchange terms for both flow and transport interaction processes. This approach is appropriate for larger problem scales due to the requirement of averaging over a representative elementary volume.

The amount and quality of available data is, for both model approaches, an essential pre-requisite for reliable model results.

Part II

Project Scale Studies